

## **Chapter 4: Results and Discussion**

### **ABSTRACT**

This chapter gives the details view of the results obtained by different characterization techniques. It is divided into six parts to explain the results of six polymers separately and exclusively.

## 4.0 RESULTS AND DISCUSSION

In this chapter the experimental results of all polymeric samples studied before and after irradiation have been reported. Polypropylene, polyimide/kapton, polyethylene terephthalate, polyether sulfone, polycarbonate/makrofol-DE and blend polymer (PVC+PET) were irradiated with 3 MeV proton beam at different fluences.

Details about all polymers are discussed in Chapter 3 (article 3.2). Descriptive view of all characterization techniques are already discussed in previous Chapter 3 (article 3.4). Effects of irradiation on physico-chemical properties for all polymers are reported here. Structural analysis was studied by FTIR spectroscopy. AC electrical properties analyzed by means of an LCR meter and changes in AC conductivity,  $\tan \delta$  (Dielectric loss), Dielectric constant was measured as a function of fluence. Thermal stability was studied by Thermogravimetric analysis (TGA); glass transition temperature ( $T_g$ ) and melting behaviour ( $T_m$ ) was studied by Differential scanning calorimetry (DSC) techniques. Mechanical property was analysed by microhardness study. Surface morphology study is also reported for all polymer samples. Possible reasons are also incorporated for these findings. This chapter is divided into six parts to explain the results of six polymers separately and exclusively.

### 4.1 Polypropylene

Polypropylene (PP) continues to be an important polymer because of its advantages in cost and performance, for health care and packaging applications. PP belongs to the family of polyolefin. It is a vinyl polymer having

hydrogen atom substituents  $(-\text{H}_2\text{C}-\text{CH}_2-)_n$  or  $(-\text{H}_2\text{C}-\text{CRH}-)_n$  and undergoes dominant homolytic rupture of the C—H bonds to form hydrogen free radicals which cross-link with each other. With increasing dose, the degree of cross-linking increases [1]. Being highly crystalline, PP exhibits high stiffness, hardness and tensile strength. It has excellent mechanical and dielectric properties. Most products made from polypropylene for medical purposes such as syringes require sterilization before use. It is the lightest known industrial polymer and finds its application in electrical appliances.

Wang et al [2] studied the effect of 100keV proton irradiation on polypropylene, which leads to cross-linking between the macromolecules of the polymer and enhancing its mechanical properties. Optical and electrical properties of 2 MeV electron and 62 MeV proton irradiated PTFE, PI, PET and PP were studied by Mishra et al [3]. The shift in optical absorption edges as observed by UV-VIS spectra of the irradiated polymers has been correlated to the optical band-gap using Tau's expression. A decrease in the optical band gap has been observed in irradiated PP and PTFE but no considerable change was found in PET and PI. Further AC conductivity measurement confirmed on increase in conductivity by electron irradiation. The effects of 23 kGy dose of 2 MeV electron irradiation on PP has been studied by Mishra et al [4] using different characterization techniques; viz FTIR spectroscopy, Electron spin resonance spectroscopy, thermogravimetric analysis, differential scanning calorimetry and X-ray diffraction analyses. Thermal stability of the polymer was found to be increasing due to electron irradiation. The isotactic nature of the polymer was found to be unaffected by electron irradiation. An increase in crystallinity of the polymer has also been observed after irradiation.

But the details study about AC frequency response, structural changes and thermal stability were not reported.

In the present work, polypropylene was irradiated with 3 MeV proton beam. The pristine and the irradiated PP at two different fluences ( $10^{13}$  and  $10^{14}$  ions/cm<sup>2</sup>) were characterized through structural, electrical, thermal and surface topography [5].

#### 4.1.1 Structural Analysis

Figure 4.1 shows the FTIR spectra of pristine and irradiated samples. The absorption bands as obtained from the pristine spectrum are identified as (A)  $984\text{ cm}^{-1}$  3/1 helix structure; (B)  $1168\text{ cm}^{-1}$  3/1 helix structure; (C)  $1296\text{ cm}^{-1}$  CH<sub>2</sub> wag; (D)  $1382\text{ cm}^{-1}$  CH<sub>3</sub> symmetric scission; (E)  $1451\text{ cm}^{-1}$  CH<sub>3</sub> asymmetric scission; (F)  $2049\text{ cm}^{-1}$  C=C alkynes group; (G)  $2838\text{ cm}^{-1}$  CH<sub>3</sub> symmetric stretching; (H)  $2906\text{ cm}^{-1}$  CH<sub>2</sub> asymmetric stretch; (I)  $2948\text{ cm}^{-1}$  CH<sub>3</sub> asymmetric stretching. It is inferred that reduction in specific height is due to deterioration of these groups in the form of H<sub>2</sub>, CO or CO<sub>2</sub>. The absorption bands representing the 3/1 helix structure of PP are found in the pristine as well as in irradiated PP at  $1168\text{ cm}^{-1}$  and  $984\text{ cm}^{-1}$  showing that the helix structure has not been affected by proton irradiation [4]. The main effect of irradiation is the formation of new bonds, free radicals, double bonds etc. The alkynes (C=C) group at  $2049\text{ cm}^{-1}$  and CH<sub>3</sub> symmetric stretching at  $2838\text{ cm}^{-1}$  are modified. The symmetric and asymmetric stretching, scissioning or bending and wagging of CH<sub>2</sub> and CH<sub>3</sub> group frequencies are modified due to irradiation. The increase in absorbance at  $2838\text{ cm}^{-1}$  in the irradiated PP can be accounted for the formation of additional CH<sub>3</sub> groups via radiation induced cross linking.

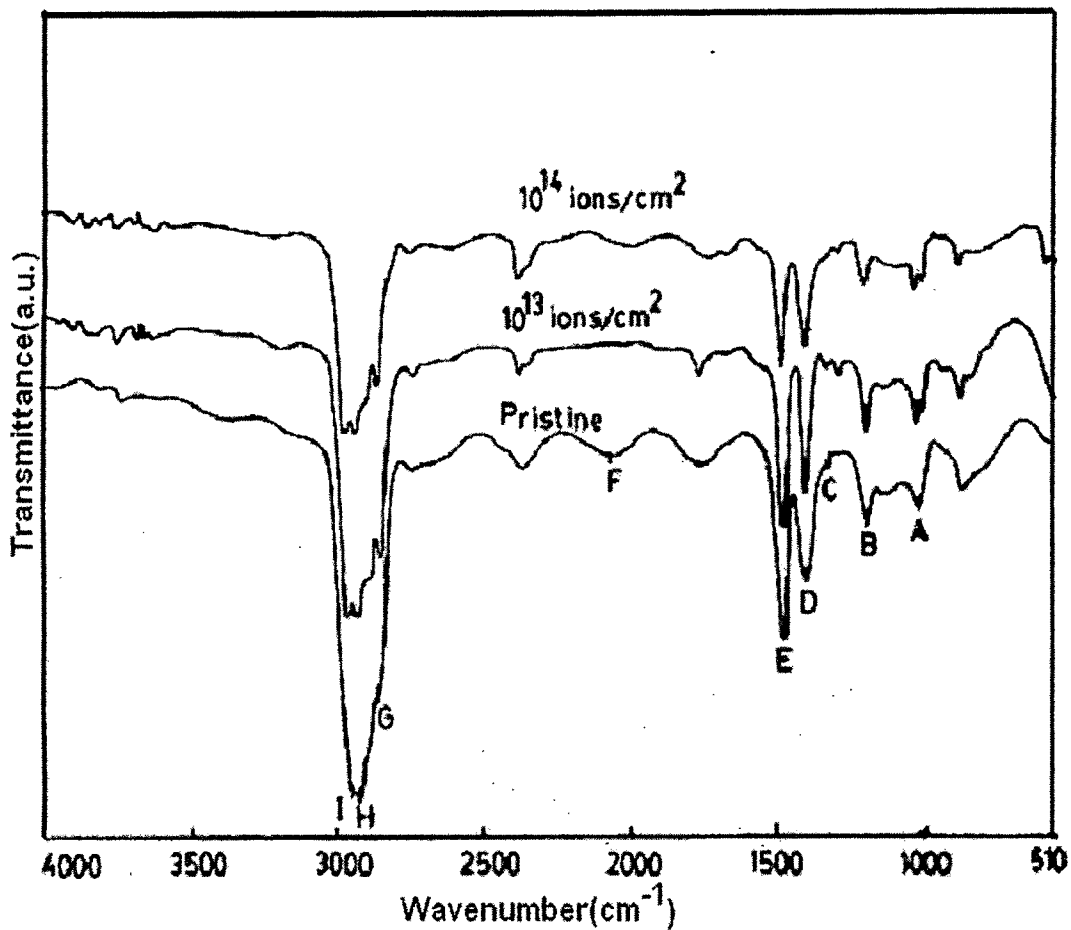


Figure 4.1: FTIR spectra for pristine and irradiated polypropylene films.

#### 4.1.2 Electrical Property

The electrical properties of pristine and irradiated polypropylene films were studied using an LCR meter. The resistance, capacitance and dielectric measurements were carried out over the frequency range 100 Hz-1MHz at room temperature. AC conductivity was calculated using equation 2.17 and dielectric constant by equation 2.19 as discussed in Chapter 2.

- **AC electrical frequency response**

The variation of conductivity with respect to log frequency ( $f$  in Hz) for pristine and irradiated samples is shown in **Figure 4.2**. A sharp increase in conductivity at 100 kHz has been observed in both cases. It is also observed that conductivity increases as fluence increases. The increase in conductivity due to irradiation may be attributed to scissioning of polymer chains and as a result increase of free radicals, unsaturation etc. An ac field of sufficiently high frequency applied to a metal polymer metal structure may cause a net polarization, which is out of phase with the field. These results in ac conductivity, it appears at frequency greater than that at which traps are filled or emptied [6].

**Figure 4.3** shows variation of  $\tan \delta$  with log  $f$  ( $f$  in Hz) for pristine and irradiated samples. It reveals that loss factor ( $\tan \delta$ ) drop sharply as frequency increases and became constant beyond a frequency of 1 kHz. It is also observed that loss factor increases as fluence increases. This indicates that loss factor ( $\tan \delta$ ) depends on frequency below 1 kHz and became constant beyond this frequency, suggesting that PP films can be used as dielectric in capacitors being used above 1 kHz frequency. It is observed that loss factor increases moderately as fluence increases. The growth in  $\tan \delta$  as the increase in conductivity is brought about by an increase in the conduction of residual current and the conduction of absorbance current [7].

**Figure 4.4** shows variation of dielectric constant ( $\epsilon$ ) with log frequency ( $f$  in Hz) for pristine and irradiated samples. The  $\epsilon$  value remains constant for low frequencies (100Hz to 100 kHz) and then decreases. At low frequencies the mobility of the free charge carrier is constant and so  $\epsilon$  is constant. As the frequency increases the charge carriers migrating through the dielectric and get

trapped against a defect sites and induce opposite charge in its vicinity, as a result of which they slow down and the value of  $\sigma$  decreases [8].

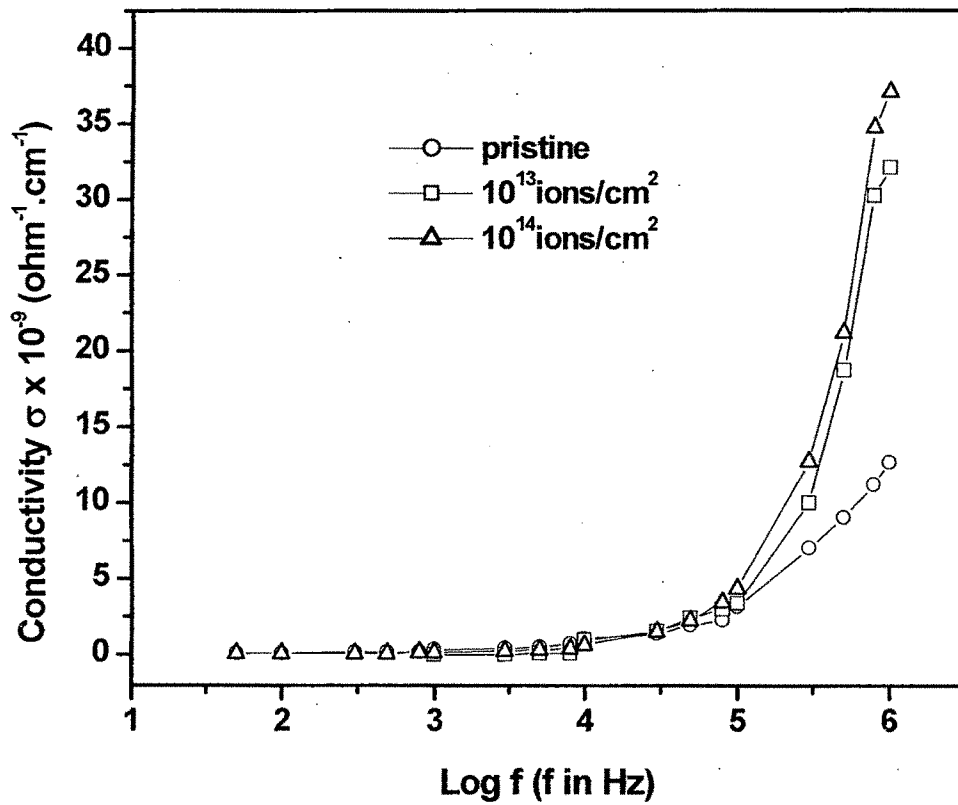


Figure 4.2: Conductivity versus Log f for pristine and irradiated polypropylene films.

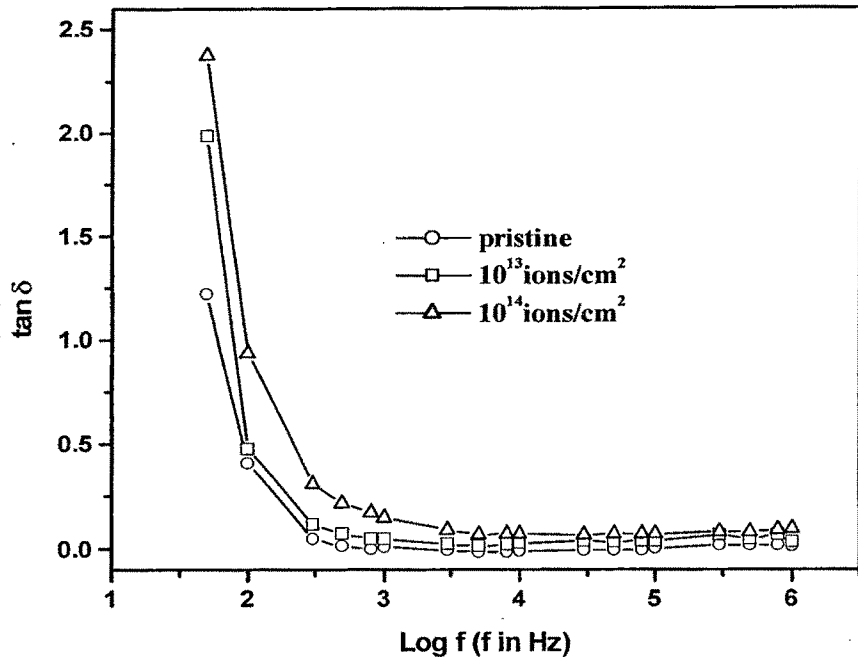


Figure 4.3:  $\tan \delta$  versus  $\text{Log } f$  for pristine and irradiated polypropylene films.

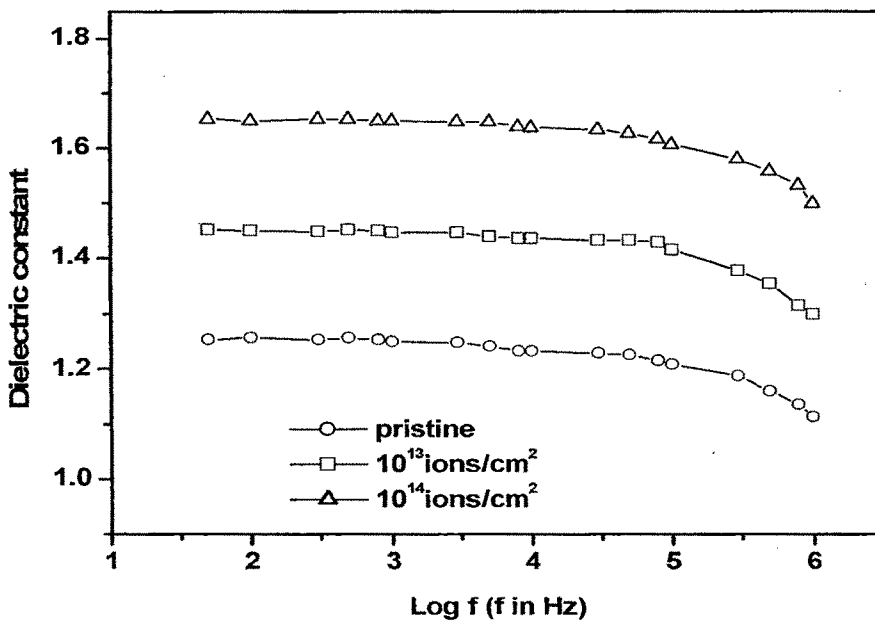


Figure 4.4: Dielectric constant versus  $\text{Log } f$  for pristine and irradiated polypropylene films.

### 4.1.3 Thermal Studies

Thermogravimetric analysis was done to study the thermal stability of the pristine and irradiated polymers.

#### 4.1.3.1 TGA analysis

The decomposition behavior of the polymer was examined by TGA as shown in **Figure 4.5**. It is quite evident from the thermo grams that there is a decrease in thermal stability due to proton irradiation. As depicted from figure, the stable zone decreases from 251°C (for pristine) to 222°C (for irradiated sample at fluence of  $10^{14}$  ions/cm<sup>2</sup>) respectively. The stable zone is followed by a slow rate of decomposition from 251-277°C for pristine and from 222-286°C for irradiated PP with weight loss (%) of about 10% and 16% respectively. A fast rate of decomposition starts after that till the sample is completely decomposed at 377 °C for pristine and 388°C for irradiated samples. It seems that irradiation changes the PP structure to some extent to make it more stable at high temperature.

The activation energy for the polymer decomposition process was calculated from the TGA thermograms using the eq<sup>n</sup>.  $\ln(\ln(m_0/m))=E/R(1/T)$ , where E is activation energy of decomposition,  $m_0$  is the initial mass, m is the mass at temperature T and R is the universal gas constant [9]. The plots of  $\ln(\ln(m_0/m))$  vs  $10^3/T$  (K<sup>-1</sup>) is shown in **Figure 4.6**. The activation energies are 69.5 kJ/mol and 63.1 kJ/mol for pristine and irradiated PP respectively. This denotes a degradation of the polymer matrix under proton irradiation, making it to start decomposition earlier than the pristine PP.

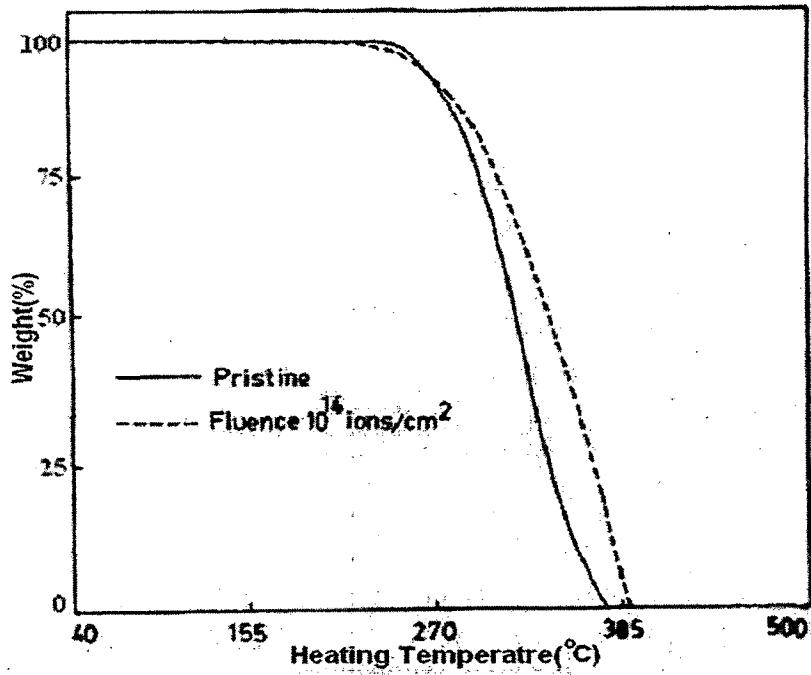


Figure 4.5: TGA thermograms for pristine and irradiated polypropylene films.

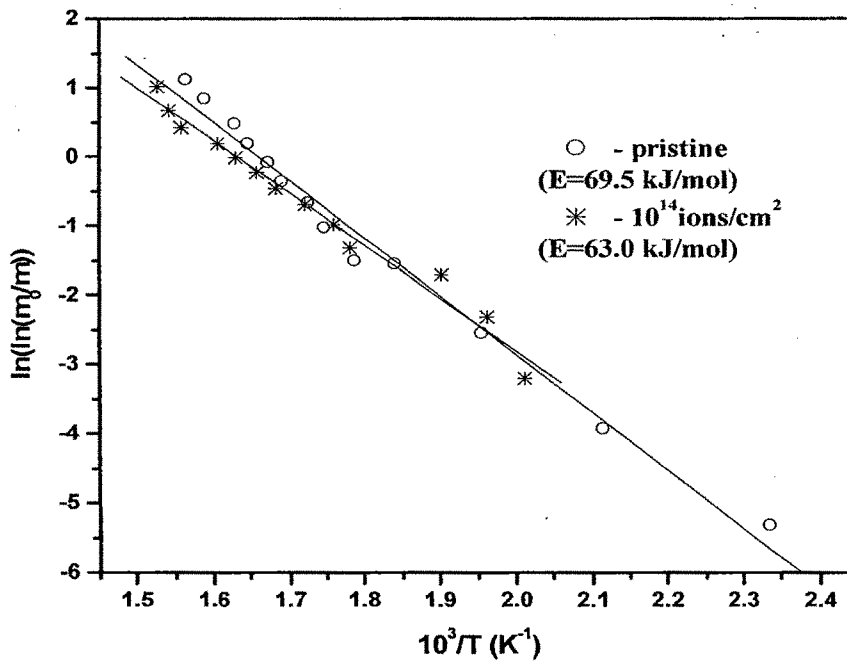


Figure 4.6:  $\ln(\ln(m_0/m))$  versus  $10^3/T$  ( $K^{-1}$ ) for the pristine and irradiated polypropylene films.

#### 4.1.4 Surface Morphology

Polypropylene is a smooth, soft and transparent. When it is exposed to proton beam, no change in color is observed. The **Figure 4.7** shows the optical micrographs of pristine and irradiated samples. It is to be noted that the irradiated samples do not appear to be flat (smooth) but seems to have the appearance of a "hill-like" contour. As the fluence increases, the size of "hill-like" contour decreases i.e. the number of hill-like contour increases. Surface of irradiated samples became rough.

#### 4.1.5 Conclusion

The general natures of FTIR spectra of pristine and irradiated polypropylene are almost same except some minor change in intensity. The irradiation gives rise the modification of C=C at  $2049\text{ cm}^{-1}$  and  $\text{CH}_3$  symmetric stretching at  $2838\text{ cm}^{-1}$ . The helix structure of PP has not been affected by proton irradiation. Proton irradiation of PP leads to chain scission and cross linking and as a result there are changes in the dielectric properties. The value of conductivity, dielectric loss and dielectric constant increases with the increase of fluence. TGA study indicates the degradation of polymer matrix under proton irradiation and making it to start decomposition earlier than the pristine PP. However, there seems to be little more stability of irradiated PP, as complete decomposition occurs at higher temperature than pristine PP. The surface of irradiated samples show "hill-like" contours as observed from optical microscope. The surface of irradiated PP films became rough compared to pristine one.

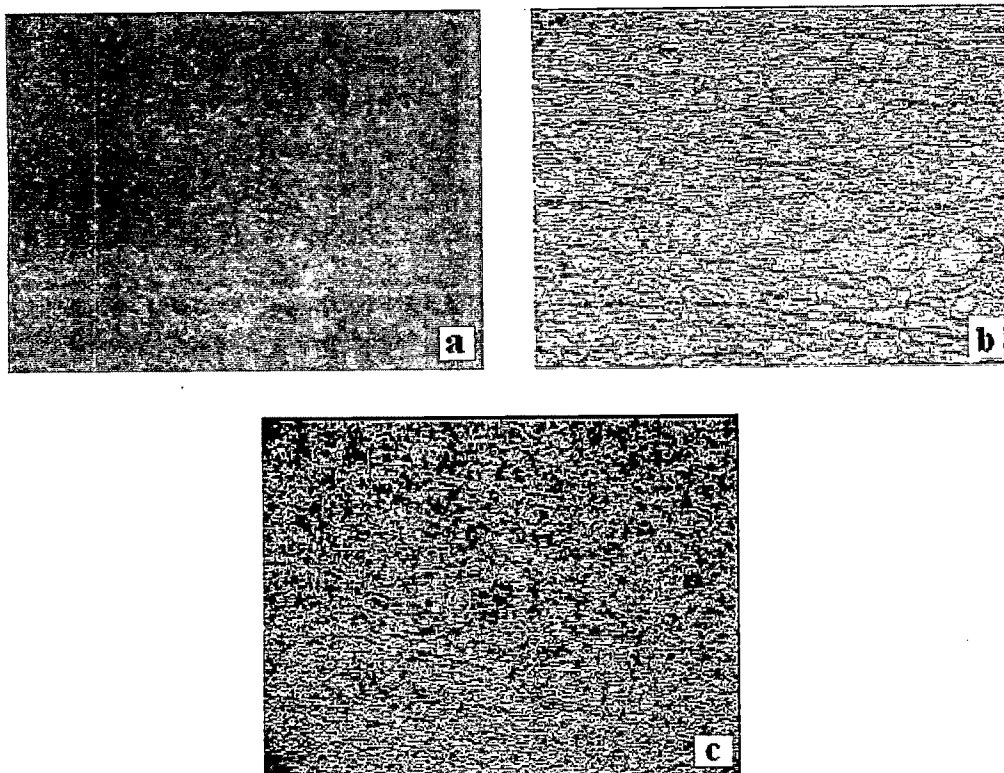


**Figure 4.7: Optical micrographs of pristine and irradiated polypropylene films; (a) pristine, (b)  $10^{13}$  ions/cm<sup>2</sup> and (c)  $10^{14}$  ions/cm<sup>2</sup>.**

## 4.2 Polyimide/Kapton

Polyimide represents an important class of high temperature, solvent resistant polymers. Aromatic heterocyclic polyimides are typical of most commercial polyimide. This polymer has such incredible mechanical and thermal properties so that they are used in place of metals and glass in many high performance applications in the electronics, automotive, and even the aerospace industries. It comes from strong intermolecular forces between polymer chains. Polyimides usually are in two forms. The first of these is linear structure where the atoms of the imide group are part of linear chain. The second of these structures is a heterocyclic structure where the imide group is part of cyclic unit in the polymer chain.

The effects of low and high energy ion beam irradiation have been studied extensively. Xu et al [10] studied ion beam induced chemical and structural modifications in PI films. The quantitative evaluation of the FTIR data shows different evolution behaviours under energetic ion irradiation for different functional groups.

Fink et al [11] investigated the IR transmission spectra for keV to MeV light and heavy ion irradiated PETP, PMMA, PC and PI films. Changes in most preexisting transmission dips have been observed as a function of the irradiation dose but no additional new IR absorption structures have been recorded after irradiation.

Terai and Kobayashi [12] studied the composition and structure changes of PI due to irradiation induced carbonization by surface characterization techniques and electric resistance measurement using 4 MeV Ni<sup>3+</sup> ions in the

fluence range  $3.5 \times 10^{12}$  to  $1.0 \times 10^{16}$  ions/cm<sup>2</sup>. They have reported that high energy ion irradiation changes the structure and the properties of PI films. High energy ion irradiation causes the carbonization of PI films effectively. In the low fluence region, the oriented structure of PI was preserved in the carbonized area, while it was destroyed with increasing fluences. The electric resistance of the film became very high in the high fluence region of  $10^{15}$  ions/cm<sup>2</sup>, which comes from the dispersion of the carbonized areas in the insulating matrix. High energy ion irradiation creates a large concentration gradient of hydrogen in the surface layer of the PI film.

Garg and Quamara [13] investigated the effects of 100 MeV Si<sup>+</sup> beam on conduction behaviour of PI. Measurements under both transient and the steady state conditions at different temperatures were made at different electric field ranging from 24 to 160 kV/cm. The loss in the carbonyl groups due to high energy ion irradiation results in a decrease of the decay rate of transient currents. The transient currents in ion irradiated samples are mainly governed by free radicals formation. Based on the Schottky coefficient estimations, the Poole Frenkel and Schottky conduction mechanism appears to be operative conduction mechanism at higher and intermediate temperature regions respectively. The decay behaviour is temperature and fluence dependent.

Virk et al [14] showed the physical and chemical response of 70 MeV carbon ion irradiated PI by using UV-visible, FTIR and XRD techniques. UV-visible spectroscopic analysis of irradiated PI revealed a change in optical density and creation of defects, which may be due to both degradation and cross linking of polymer chains simultaneously. FTIR analyses revealed that ring

or ladder-structured polymers are chemically highly resistant to electronic energy loss. PI has partial crystallinity as evidenced by XRD patterns.

Mishra et al [15] studied the spectroscopic and thermal behaviour of 2 MeV electron irradiated PI by using FTIR spectroscopy, TGA and DSC measurement. Through emergence of any new structures after irradiation was not observed, yet a decrease in thermal stability of the polymer accompanied by decrease in melting temperature was observed after irradiation.

In the present work, PI films were irradiated with 3 MeV proton beam at the fluences of  $10^{13}$ ,  $10^{14}$  and  $10^{15}$  ions/cm<sup>2</sup>. Pristine and irradiated kapton films were characterized through structure, electrical, thermal, mechanical and surface morphology [16,17].

#### 4.2.1 Structural Analysis

The FTIR spectra of pristine and irradiated Polyimide (PI) samples are shown in **Figure 4.8**. The absorption bands as obtained from the pristine spectrum are identified as (A) 932 cm<sup>-1</sup>: C-C stretching vibration; (B) 1015 cm<sup>-1</sup>: C-O-C stretching of ester; (C) 1728 cm<sup>-1</sup>: C=O stretching vibration; (D) 2777 cm<sup>-1</sup>: C-H stretching vibration; (E) 3073 cm<sup>-1</sup>: aromatic C-H stretching vibration; (F) 3486 cm<sup>-1</sup>: C-H bending vibration; (G) 3630 cm<sup>-1</sup>: O-H stretching vibration. C=O (Carbonyl group) is prone to irradiation and intensity of C=O group decreases. It is observed from the comparison of the spectra of pristine and irradiated samples that no significant change in the vibrational frequencies occurs. This implies that the inter-chain separation is not affected much by proton beam irradiation. Most of the peak positions were found unchanged. There is no

change in the overall structure of the polymer. It may be concluded that polyimide is highly resistant to radiation degradation.

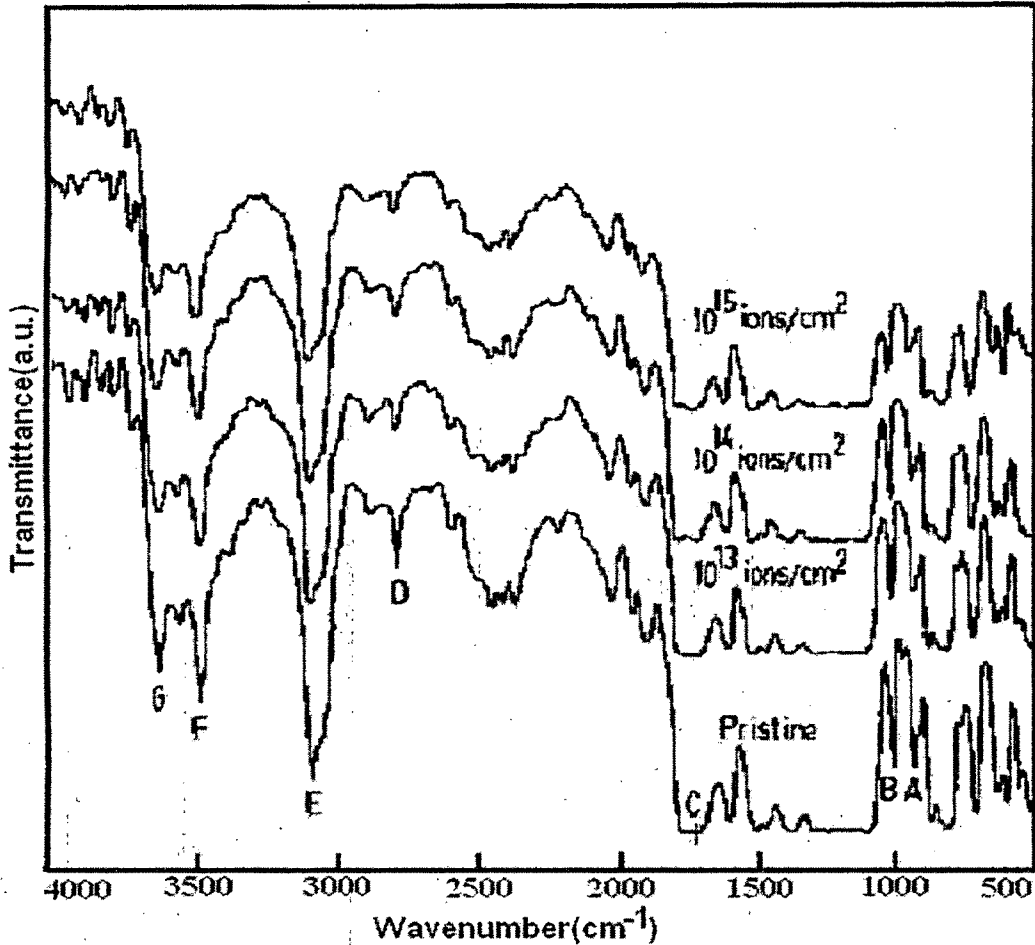


Figure 4.8: FTIR spectra for pristine and irradiated polyimide/kapton films.

#### 4.2.2 Electrical Property

Electrical properties of pristine and irradiated samples were studied using an LCR meter in the frequency range 100 Hz-100kHz. The resistance, capacitance and dielectric loss measurements were carried out at ambient temperature. AC conductivity was calculated using equation 2.17 and dielectric constant by equation 2.19 as discussed in Chapter 2.

- **AC electrical frequency response**

The **Figure 4.9** shows the variation of conductivity with log frequency ( $f$  in Hz) for the pristine and irradiated polyimide films. A sharp increase in conductivity has been observed around 50 kHz for pristine and irradiated samples. It is also observed that the conductivity increases as fluence increases. The increase in conductivity due to irradiation may be attributed to scissioning of the polymer chains and resulting in an increase of free radicals, unsaturation, etc. An AC field of sufficiently high frequency applied to a metal-polymer-metal structure may cause a net polarization, which is out of phase with the field. This results in AC conductivity; it appears at frequencies greater than that at which traps are filled or emptied [6].

**Figure 4.10** shows the plot of  $\tan \delta$  versus log frequency for the pristine and irradiated samples. It is observed that loss factor ( $\tan \delta$ ) increases moderately as frequency increases up to 10 kHz. It is also observed that the loss factor increases as the fluence increases.  $\tan \delta$  has positive values indicating the dominance of inductive behavior.

**Figure 4.11** shows the variation of dielectric constant with log frequency for the pristine and irradiated samples. As evident from the graph the dielectric constant remains almost constant over a wide frequency range and increases as the fluence increases. It is an interesting observation because lot of Kapton based capacitors are used in nuclear plants and bound to be exposed to nuclear radiation.

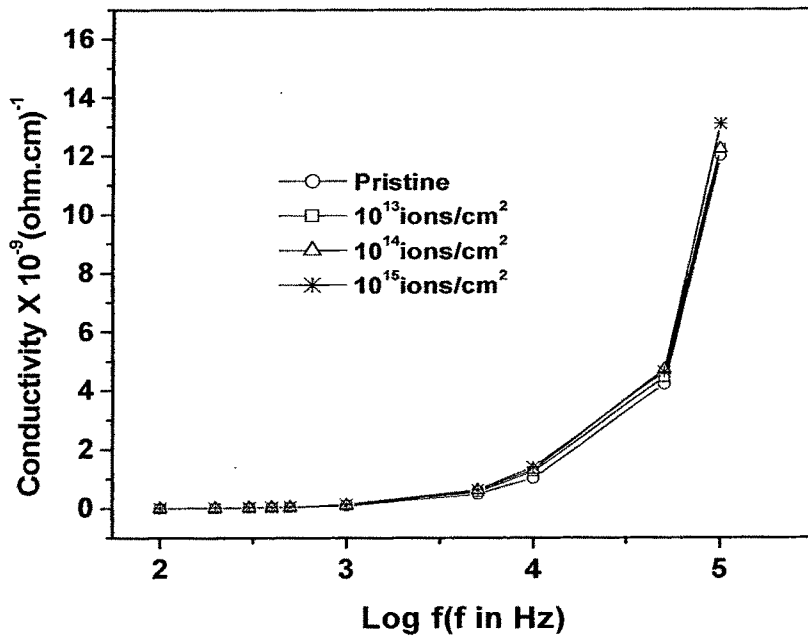


Figure 4.9: Conductivity versus Log f for pristine and irradiated polyimide/kapton films.

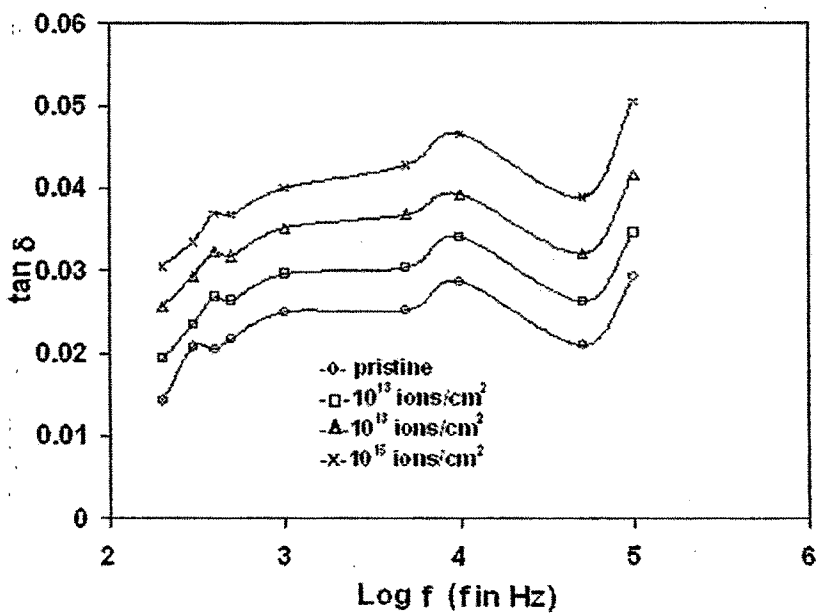


Figure 4.10:  $\tan \delta$  versus Log f for pristine and irradiated polyimide/kapton films.

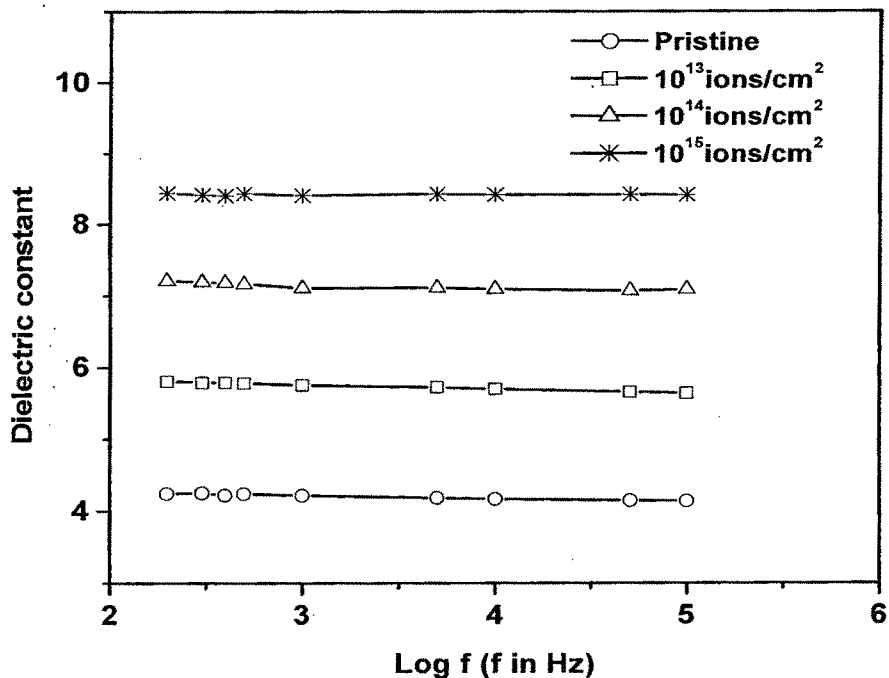


Figure 4.11: Dielectric Constant versus Log f for pristine and irradiated polyimide/kapton films.

### 4.2.3 Thermal Studies

The thermal response of the pristine and irradiated kapton samples was verified by two techniques, viz. (i) thermogravimetric analysis and (ii) differential scanning calorimetry.

#### 4.2.3.1 TGA analysis

The TGA thermograms of pristine and irradiated PI samples are shown in Figure 4.12. The pristine sample was completely stable up to 410°C, where there is no weight loss of the sample. This zone is followed by a slow rate of decomposition. Due to the limited heating temperature of up to 500°C, the weight loss of about 12% for pristine and 18% for irradiated ( $10^{15}$  ions/cm<sup>2</sup>) PI

was observed. The stable zone of irradiated sample was observed up to the temperature of 395°C.

#### 4.2.3.2 DSC analysis

Figure 4.13 shows the DSC thermograms for the pristine and irradiated PI samples. The glass transition temperature ( $T_g$ ) was observed around 265°C in pristine, and no significant change was observed in irradiated ( $10^{14}$  ions/cm<sup>2</sup>) sample. As the DSC study was done in temperature range 40°C-325°C, no melting temperature ( $T_m$ ) was obtained.

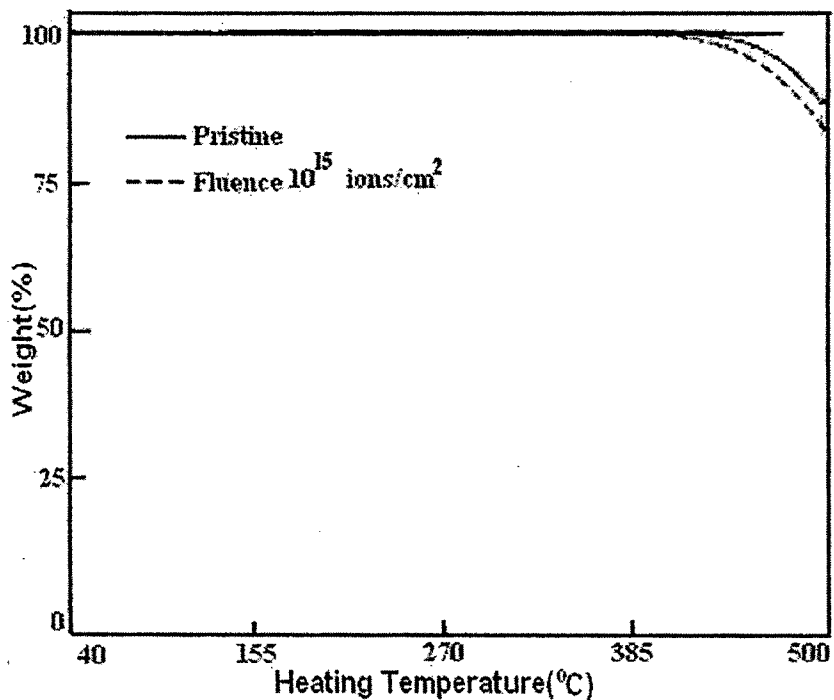
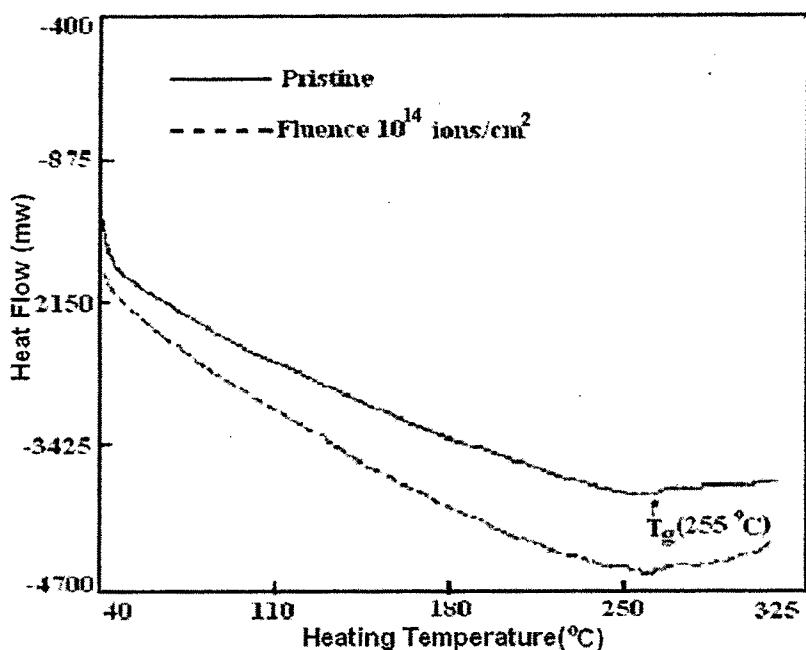


Figure 4.12: TGA thermograms for pristine and irradiated polyimide/kapton films.



**Figure 4.13: DSC thermograms for pristine and irradiated polyimide/kapton films.**

#### **4.2.4 Mechanical Property (microhardness)**

We have studied the mechanical property (microhardness) by means of Vickers' microhardness tester. The Vickers' hardness was calculated using equation 2.4 as discussed in Chapter 2.

**Figure 4.14** gives the plots of the Vickers' microhardness (Hv) versus applied load P, at different fluences. It is evident that the hardness value increases with load up to 300 mN and then saturates beyond the load of 400 mN. The increase of Hv with load can be explained on the basis of the strain-hardening phenomenon. On applying the load, the polymer is subjected to some strain hardening. Beyond certain load the polymer exhausts its strain hardening capacity and the hardness tends to become constant.

The rate of strain hardening is greater at low loads and decreases at higher loads [18,19]. As can be seen, the hardness becomes independent of load for more than 400 mN. The value obtained from the saturation region, therefore, represents the true hardness of the bulk material, since at high loads the indenter penetration depth is also high and surface effects become insignificant. It is also observed that the hardness increases as fluence increases. This may be attributed to the cross linking phenomenon [18].

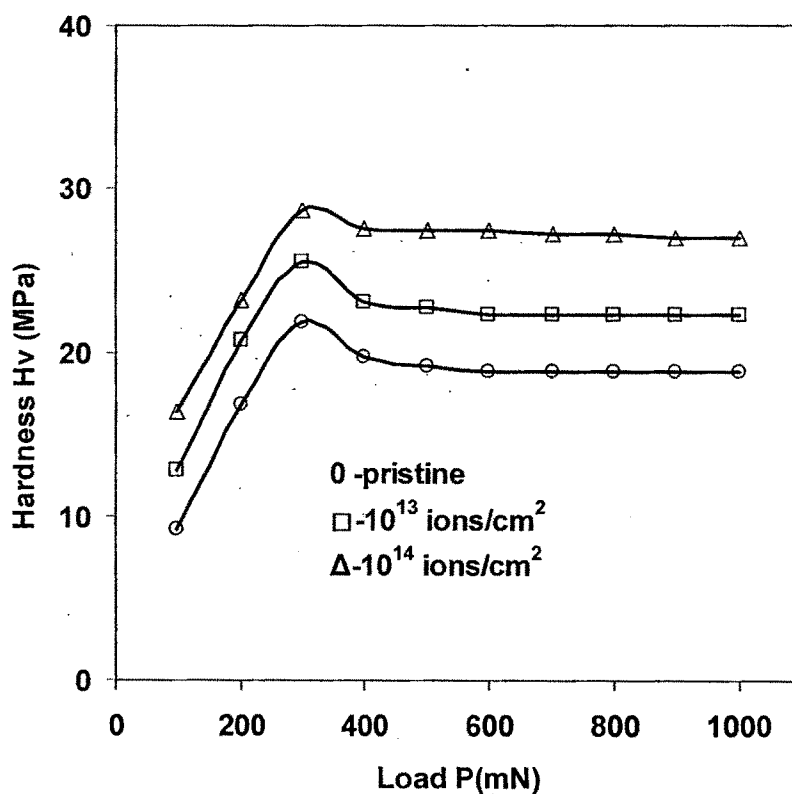


Figure 4.14: Microhardness for pristine and irradiated polyimide/kapton films.

#### 4.2.5 Surface Morphology

Polyimide/kapton is a semi transparent and yellowish brown (amber) in color. When it is irradiated with the proton beam of fluence  $10^{13}$ - $10^{15}$  ions/cm<sup>2</sup>; no change in its color is observed by naked eye. When these samples were studied by optical microscope, its colour changes have been observed. **Figure 4.15** shows the optical micrographs of pristine and irradiated samples. It is observed that the surfaces of irradiated samples do not appear to be flat (smooth). It became rough and the roughness increases as fluence increases.

#### 4.2.6 Conclusion

It is observed from the comparison of FTIR spectra of pristine and irradiated polyimide that no significant change has been observed in the overall structure of the polymer but minor changes observed in the intensity of irradiated samples as compared to the pristine which may be due to the breakage of a few bonds. It is also revealed from thermal analysis that PI is highly resistant to radiation degradation. The value of conductivity, dielectric loss and dielectric constant were observed to increase with the increase of fluence. This may be attributed to scissioning of polymeric bonds, resulting in an increase of free radicals, unsaturation etc. Proton irradiation has been found to increase the Vickers' hardness of the Kapton films. It is observed from the optical micrographs that the irradiated samples do not appear to be flat (smooth). It became rough and the roughness of surface increases as the fluence increases.

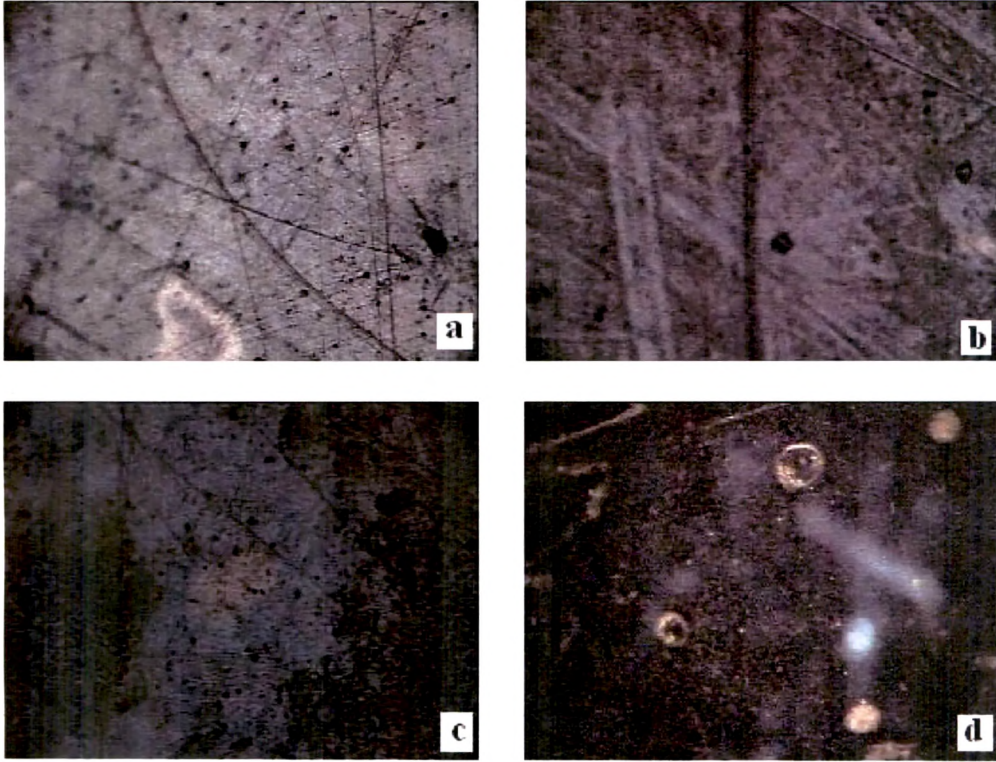


Figure 4.15: Optical micrographs for pristine and irradiated polyimide/kapton films (a) pristine, (b)  $10^{13}$  ions/cm<sup>2</sup>, (c)  $10^{14}$  ions/cm<sup>2</sup> and (d)  $10^{15}$  ions/cm<sup>2</sup>.

### 4.3 Polyethylene terephthalate

Polyethylene terephthalate (PET) is a soft, transparent thermoplastic with a high melting point (~265 °C) and a very good mechanical strength (at least up to 175 °C) due to the presence of the aromatic ring in the polymeric structure. It is resistant to heat and moisture and virtually immune to many chemicals and has wide applications.

The effects of ion beam irradiation on PET have been studied extensively by number of author using keV-MeV, light and heavy ions.

Ciesla and Starosta [20] reported the DSC, FTIR and XRD studies on PET films irradiated with high energy heavy ions at high fluences. DSC revealed the amorphization of PET films after heavy ion irradiation. Differences in melting and crystallization processes between pristine and irradiated samples were observed on primary heating but also on cooling and repeated heating. The decrease in crystallinity was confirmed by wide and small angle XRD and volume crystallinity measurements. The amorphization is due to cross linking and degradation process. The changes in irradiated PET revealed by IR spectroscopy can also be attributed to an increase of the content of amorphization phase.

Steckenreiter et al [21] showed the chemical modification of PET induced by swift heavy ions. The irradiations with Kr (8.6 MeV/u) and with Mo (5.6 MeV/u) ions were performed under vacuum and in oxygen atmosphere, respectively. The overall degradation of polymer was investigated as a function of fluence. A significant loss of crystallinity is related to scission processes of the main chains at the ethylene glycol residue. The benzene ring structure show

only small changes under irradiation and do not seem to participate in the degradation process significantly. While various degradation processes known from photochemical degradation take place, the creation of alkynes near the track core is found to be a unique process induced by heavy ions. The presence of oxygen during irradiation enhances the overall degradation of PET leads to enhanced formation of alkynes and CO<sub>2</sub>.

Biswas et al [22] studied the effect of swift heavy ion irradiation on the radiochemistry and melting characteristics of PET by FTIR and DSC techniques. After irradiation with a 180 MeV Ag<sup>14+</sup> ion beam, DSC measurements of PET films exhibited significant change in their melting behaviour. The gradual increase in the melting enthalpy of irradiated PET with the ion fluence is observe, which reaches a maximum when track overlapping sets in, and decreases exponentially thereafter. FTIR measurements of irradiated PET at different ion fluences have also shown partly different trend of amorphisation. X-ray diffractions results of irradiated PET revealed a shift and a reduction of the main peak along with the appearance of a new small peak.

Tripathy et al [23] studied 62 MeV proton induced modification in polyethylene terephthalate by using FTIR spectroscopy, thermogravimetric analysis, differential scanning calorimetry, and X-ray diffraction spectroscopy. The experiments revealed a restoration of the crystalline matrix and simultaneous decrease in thermal stability in the irradiated polymer as a function of dose, indicating that PET underwent both degradation and cross lining by proton irradiation.

However, detailed study of change in microhardness and electrical property due to ion irradiation has not much been reported. In this work we have

reported the effects of 3 MeV proton on the electrical, mechanical, thermal and surface morphology of PET at different fluences. The changes in these properties of polymer have been corroborated with structural modifications as observed with the FTIR spectroscopy.

Pristine and irradiated PET films were characterized through structural (FTIR spectroscopy), electrical (LCR meter), thermal (TGA and DSC), mechanical (microhardness tester) and surface topography [24,25].

### 4.3.1 Structural Analysis

The FTIR spectra of the pristine and irradiated samples are shown in **Figure 4.16**. The absorption bands as obtained from the pristine spectrum are identified as: (A)  $725\text{ cm}^{-1}$ : ring deformation of phenyl ring, bending vibration of  $\text{CH}_2$  group; (B)  $862\text{ cm}^{-1}$ : C-H deformation of phenyl ring, vibration band of para substituted benzene ring; (C)  $1730\text{ cm}^{-1}$ : C = O stretching vibration; (D)  $2335\text{ cm}^{-1}$ : vibration of  $\text{CO}_2$ ; (E)  $2975\text{ cm}^{-1}$ : C-H stretching of  $\text{CH}_2$  group; (F)  $3068\text{ cm}^{-1}$ : C-H stretching aromatic group; (G)  $3294\text{ cm}^{-1}$ : C-H stretching vibrations of the alkyne group. Steckenreiter et al [21] also reported a band at  $3294\text{ cm}^{-1}$  which is assigned to the characteristic C-H stretching mode of the alkynes end group (R-C≡C-H). The formation of the alkyne groups is also confirmed by the simultaneous observation of the C=C stretching vibration band at  $2102\text{ cm}^{-1}$ . The bands in the wave number region from  $3600\text{ cm}^{-1}$ - $2500\text{ cm}^{-1}$  are due to the O-H stretching vibration. The band at  $1504\text{ cm}^{-1}$ , corresponds to amorphisation of the crystalline fraction and main chain scission at the para position of distributed benzene rings [22]. It is observed that there is no change in overall structure of the polymer but a minor change in intensities have been observed

up to the fluence of  $10^{14}$  ions/cm<sup>2</sup>. This might be due to the breakage of a few bonds in the structure. It may be concluded that PET is resistant to radiation at least up to the fluence of  $10^{14}$  ions/cm<sup>2</sup>. The spectrum corresponding to the fluence of  $10^{15}$  ions/cm<sup>2</sup> indicates a very significant change in the structure of polymer. This might be due to the scissioning of polymer chain. Further at this fluence, there was severe surface roughening (as observed by optical microscope) and became opaque. There is a drastic fall in the transmitted intensity due to scattering of IR beam from the surface.

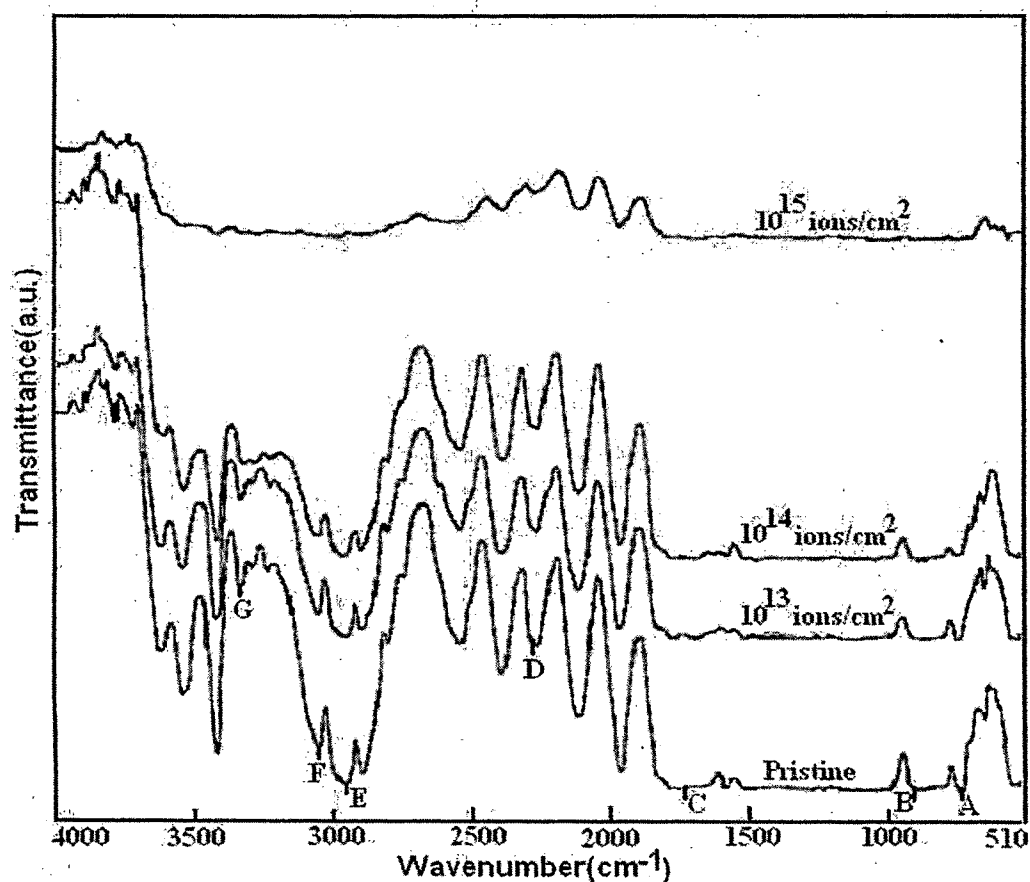


Figure 4.16: FTIR spectra for pristine and irradiated polyethylene terephthalate films.

### 4.3.2 Electrical Property

Electrical properties of pristine and irradiated samples were studied using an LCR meter in the frequency range 100 Hz to 1MHz. The resistance, capacitance and dielectric loss measurements were carried out at ambient temperature. AC conductivity was calculated using equation 2.17 and dielectric constant by equation 2.19 as discussed in Chapter 2.

- **AC electrical frequency response**

**Figure 4.17** shows the variation of electrical conductivity with log of frequency for the pristine and irradiated PET films. A sharp increase in conductivity has been observed around 300 kHz for pristine and irradiated samples. It is also observed that conductivity increases as fluences increases. The increase in conductivity due to irradiation may be attributed to scissioning of polymer chains and as a result increase of free radicals, unsaturation etc. An ac field of sufficiently high frequency applied to metal-polymer-metal structure may cause a net polarization, which is out of phase with the field. This results in ac conductivity, it appears at frequency greater than that at which traps are filled or emptied [6].

**Figure 4.18** shows a plot of  $\tan \delta$  versus log of frequency for pristine and irradiated samples in the frequency range 300 Hz to 1 MHz. It is observed that the variation of  $\tan \delta$  with log frequency is identical for pristine and irradiated samples at low frequencies, and higher for irradiated samples. This possibly indicates the dominance of inductive behavior. The  $\tan \delta$  decreases as frequency increases and becomes negative beyond a frequency of 300 kHz for

pristine and irradiated sample up to the fluence of  $10^{14}$  ions/cm<sup>2</sup>. This shows dominance of capacitive contributions [26].

Figure 4.19 shows the variation of dielectric constant with log frequency for the pristine and irradiated samples. As evident from the plot, the dielectric constant remains almost constant up to 100 kHz and then decreases at higher frequencies. At low frequencies, the mobility of the free charge carriers is constant and thus the dielectric constant remains unchanged. As the frequency increases, the charge carriers migrating through the dielectric and get trapped at defect sites and induce an opposite charge in its vicinity, as a result of which they slow down and the value of dielectric constant decreases. At these frequencies, the polarization of trapped and bound charges can not take place and hence the dielectric constant decreases.

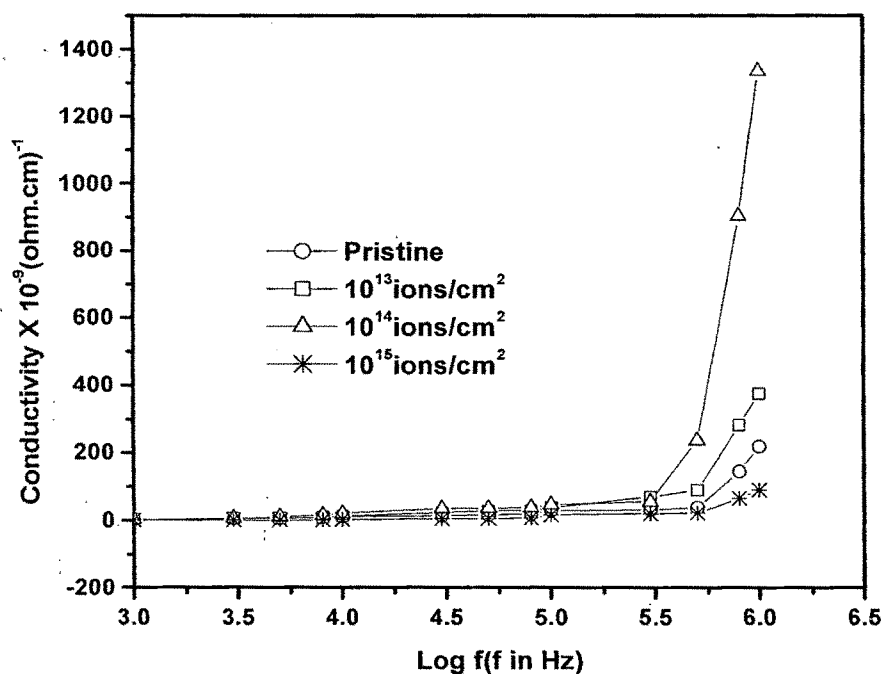


Figure 4.17: Conductivity versus Log f for pristine and irradiated polyethylene terephthalate films.

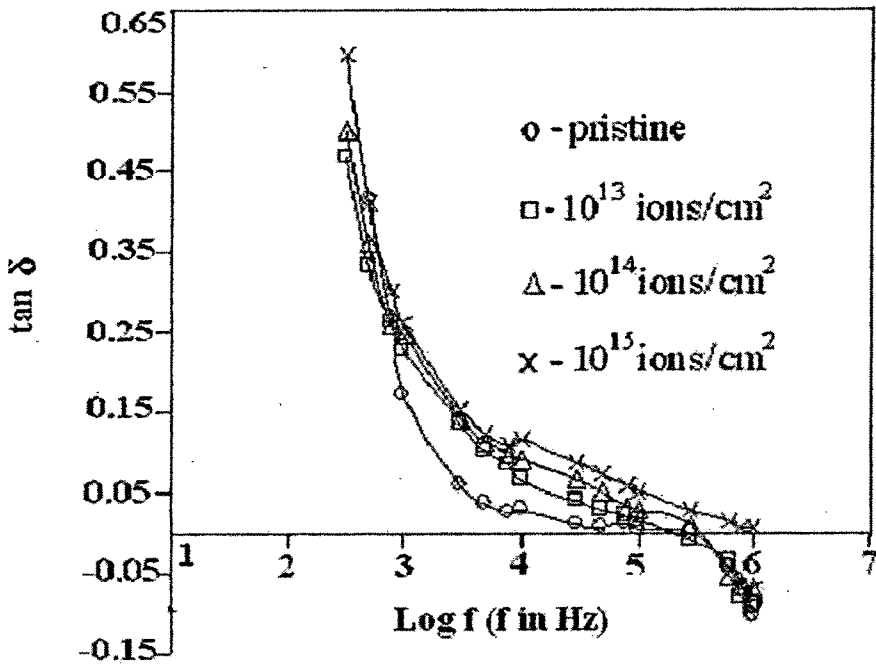


Figure 4.18:  $\tan \delta$ , versus  $\text{Log } f$  for pristine and irradiated polyethylene terephthalate films.

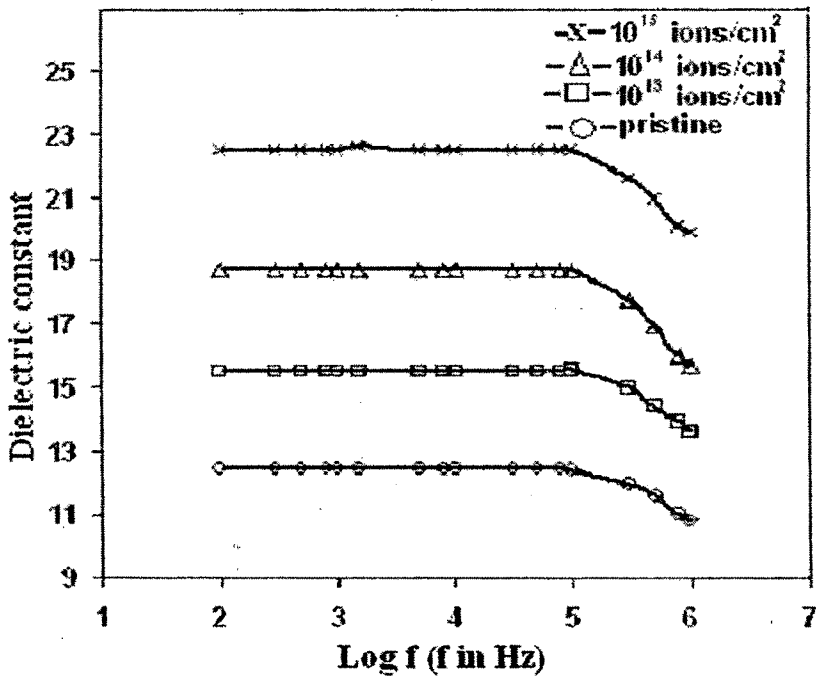


Figure 4.19: Dielectric constant, versus  $\text{Log } f$  for pristine and irradiated Polyethylene terephthalate films.

### 4.3.3 Thermal Studies

Thermogravimetric analysis and differential scanning calorimetry were done to characterize the pristine and the irradiated PET films.

#### 4.3.3.1 TGA analysis

The TGA thermograms of pristine and irradiated samples are shown in **Figure 4.20**. As depicted in the figure the stable zones for pristine and irradiated (at the fluence of  $10^{14}$  ions/cm<sup>2</sup>) samples are the same (up to the temperature of 222°C) though at the fluence of  $10^{15}$  ions/cm<sup>2</sup>, the stable zone is present only up to 127°C. This change clearly indicates that up to the fluence of  $10^{14}$  ions/cm<sup>2</sup>, the system remains reasonably organized but gets quite disorganized with some residual energy when fluence of  $10^{15}$  ions/cm<sup>2</sup> is used. Some bond formation, i.e., forming a more organized structure seems to occur up to the fluence of  $10^{14}$  ions/cm<sup>2</sup>. The weight loss of 0.8 %, 1.5 % and 4.6 % has been observed for the pristine and irradiated samples at  $10^{14}$  and  $10^{15}$  ions/cm<sup>2</sup>, respectively, at the temperature of 343°C. However, at the temperature of 383°C, the weight loss of 3.9 % has been observed for pristine and irradiated samples (at the fluence of  $10^{14}$  ions/cm<sup>2</sup>), whereas at the fluence of  $10^{15}$  ions/cm<sup>2</sup> a weight loss of 10% is observed. From the data, it is evident that no significant change has been observed up to the fluence of  $10^{14}$  ions/cm<sup>2</sup>, the fact also revealed by FTIR Spectra (**Figure 4.16**).

The activation energy for the polymer decomposition process was calculated from the TGA patterns using the equation [9].

$$\ln\left[\ln\left(\frac{m_0}{m}\right)\right] = -\frac{E}{R}\left(\frac{1}{T}\right) + \text{const} \quad , \quad \text{where } E \text{ is the activation energy of}$$

decomposition,  $m_0$  is the initial mass,  $m$  is the mass at temperature  $T$  and  $R$  is the universal gas constant. The plots of  $\ln [\ln (m_0/m)]$  versus  $10^3/T$  are shown in **Figure 4.21**. It is observed that up to the fluence of  $10^{14}$  ions/cm<sup>2</sup>, the system remains reasonably organised but gets quite disorganised with some residual energy when fluence of  $10^{15}$  ions/cm<sup>2</sup> is used. Some bond formation, i.e. formation of a more organised structure, seems to be happening up to the fluence of  $10^{14}$  ions/cm<sup>2</sup> as indicated by higher  $E$  of decomposition (260 kJ/mol) at  $10^{14}$  ions/cm<sup>2</sup>. However, decomposition is facilitated at higher fluence (i.e.  $10^{15}$  ions/cm<sup>2</sup>,  $E=127$  kJ/mole). The activation energy for pristine PET sample is 216 kJ/mol.

#### **4.3.3.2 DSC Analysis**

Figure 4.22 shows, the DSC curves for pristine and irradiated PET films at the fluence of  $10^{13}$  and  $10^{14}$  ions/cm<sup>2</sup>. It is observed that the endotherm denoting the melting temperature ( $T_m$ ) underwent a change after irradiation. The endotherm for the pristine PET was observed at 262°C. By increasing the ion fluence up to  $10^{14}$  ions/cm<sup>2</sup>, the radiation damage effects on PET became more evident, and the melting endotherm ( $T_m$ ) is shifted to lower temperature up to ~ 248°C. From the analyses of DSC curves, the enthalpy of melting endotherm can be considered as the overlap of two distinct terms, one at higher temperature corresponds to less damaged material compared to low temperature peaks [27]. The decrease in melting temperature with fluence

further support the fact that scissioning of chemical bonds predominate by proton irradiation.

#### 4.3.4 Mechanical Property (microhardness)

We have studied the mechanical property (microhardness) by means of Vickers' microhardness tester. The Vickers' hardness was calculated using equation 2.4 as discussed in Chapter 2.

Figure 4.23 shows the plot of Vickers' microhardness ( $H_V$ ) versus applied load ( $P$ ) obtained for the pristine and irradiated samples.

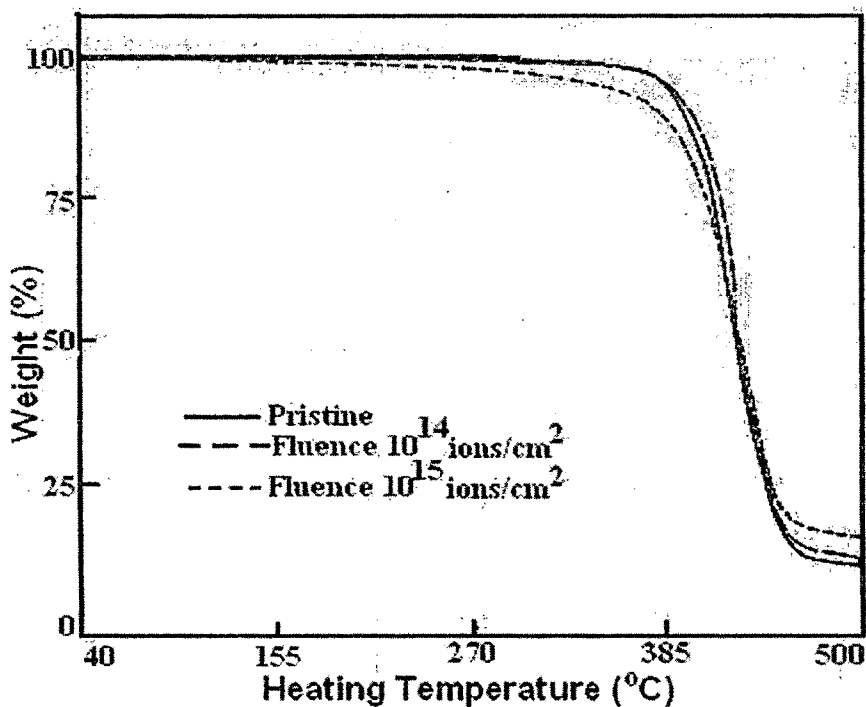


Figure 4.20: TGA thermograms for pristine and irradiated polyethylene terephthalate films.

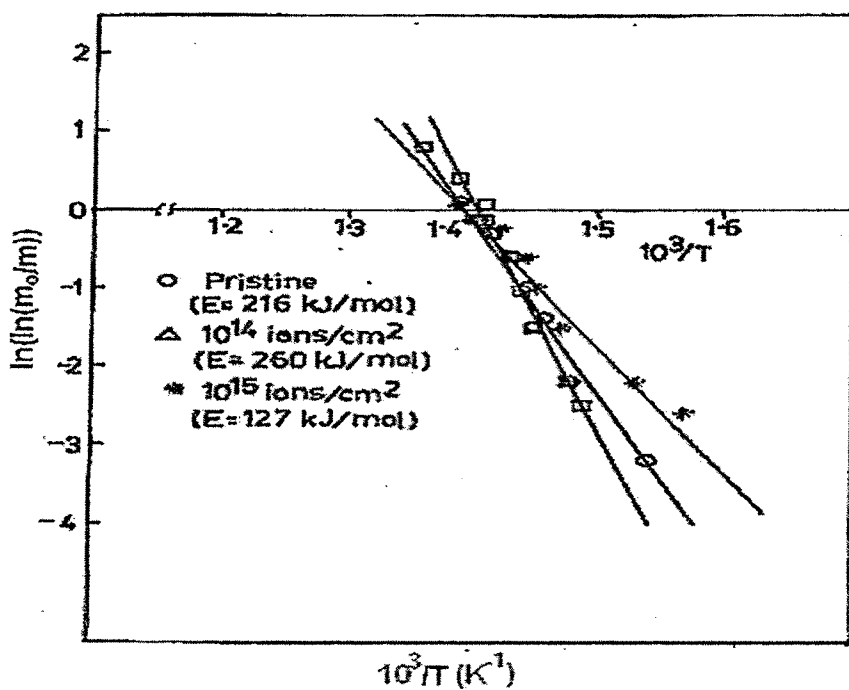


Figure 4.21:  $\ln(\ln(m_0/m))$  versus  $10^3/T$  ( $K^{-1}$ ) for the pristine and irradiated polyethylene terephthalate films.

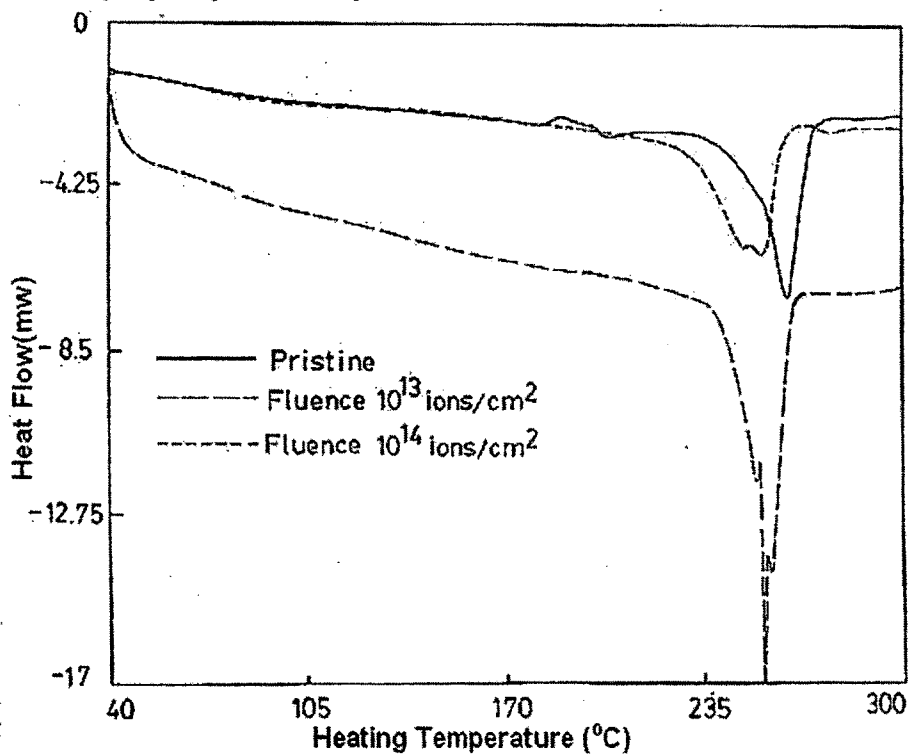


Figure 4.22: DSC thermograms for pristine and irradiated polyethylene terephthalate films.

It is evident from the figure that the microhardness is maximum at the fluence of  $10^{14}$  ions/cm<sup>2</sup>. The increase in the hardness may be attributed to the cross linking effect [18]. The hardness is known to be influenced by surface effects. Particularly at low penetration depths, the strain hardening modifies the true hardness of the material. At the higher loads beyond 400 mN, the interior of the bulk specimen is devoid of surface effects. Hence, the hardness value at higher loads represents the true value of the bulk and it is consequently independent of the load. The hardness is seen to increase as fluence increases up to the fluence of  $10^{14}$  ions/cm<sup>2</sup>. However, with increasing fluence, the polymer degrades its mechanical strength and as a result hardness decreases at the fluence of  $10^{15}$  ions/cm<sup>2</sup>. The degradation may be a result of scissioning of the chemical bonds at the higher radiation fluences. It is also observed from FTIR spectra that structure of polymer changed at the fluence of  $10^{15}$  ions/cm<sup>2</sup>.

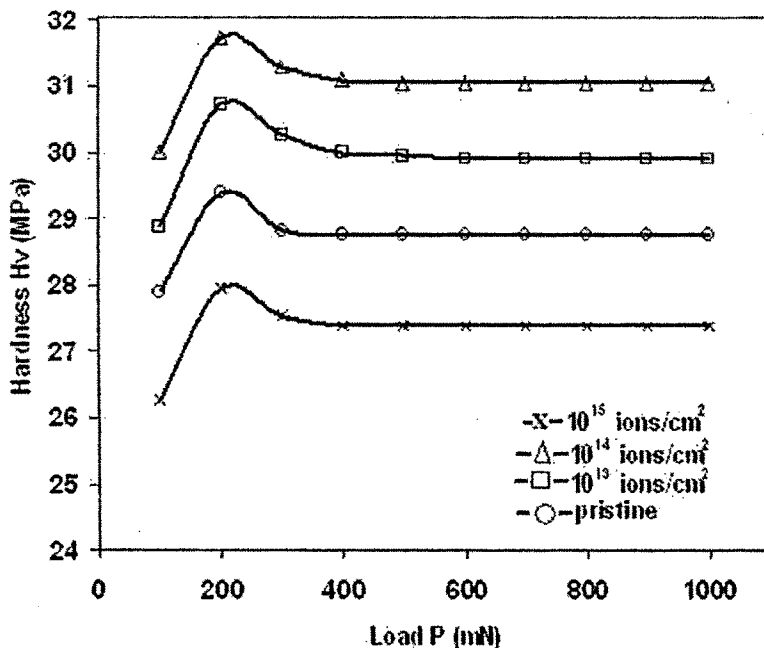


Figure 4.23: Microhardness for pristine and irradiated polyethylene terephthalate films.

### 4.3.5 Surface Morphology

Polyethylene terephthalate is milky white with shiny and smooth surface. The modification of polymer surface is found with the change in the colour of the polymer which is white milky with shiny for the pristine film and no appreciable change in colour has been observed at the fluence of  $10^{13}$  ions/cm<sup>2</sup>. On the further increase of the fluence the surface became light-yellowish, and yellowish-brown at the fluence of  $10^{14}$  and  $10^{15}$  ions/cm<sup>2</sup> respectively. When these polymers were observed through optical microscope as shown in **Figure 4.24**, it is to be noted that the irradiated samples do not appear to be flat (smooth), but seem to be rough. The roughness of the samples increases as fluence increases.

### 4.3.5 Conclusion

The FTIR spectra indicate that PET gets chemically degraded at the highest proton fluence used that is  $10^{15}$  ions/cm<sup>2</sup>. It is observed that there are no changes in overall structure of the polymer but a minor change in intensities have been observed up to the fluence of  $10^{14}$  ions/cm<sup>2</sup>. This might be breakage of few bonds in the structure. There is an exponential increase in conductivity with log of frequency and the effect is significant at higher fluences. The loss factor (tan  $\delta$ ) and dielectric constant are observed to change appreciably with the fluences. The calorimetric measurements of 3 MeV proton irradiated PET show significant change in melting enthalpy and it decreases as fluence increases. This decrease in melting temperature is attributed to the decrease in molecular weight. The minor changes have been observed due to the cross-

linking and scissioning of the irradiated PET as evidenced from TGA and DSC thermograms. However, chain scission by proton irradiation at higher fluence seems to be the dominant process. The Vickers hardness of the polymer increases up to a fluence of  $10^{14}$  ions/cm<sup>2</sup>, probably due to cross-linking without any degradation effect. However, the hardness decreases at the fluence of  $10^{15}$  ions/cm<sup>2</sup> because of degradation of the polymer due to scissioning of bonds; which is also corroborated with the FTIR spectra. It is observed from the optical micrographs; that the irradiated samples do not appear to be flat (smooth). It became rough and the roughness of polymer surface increases as the fluence increases.

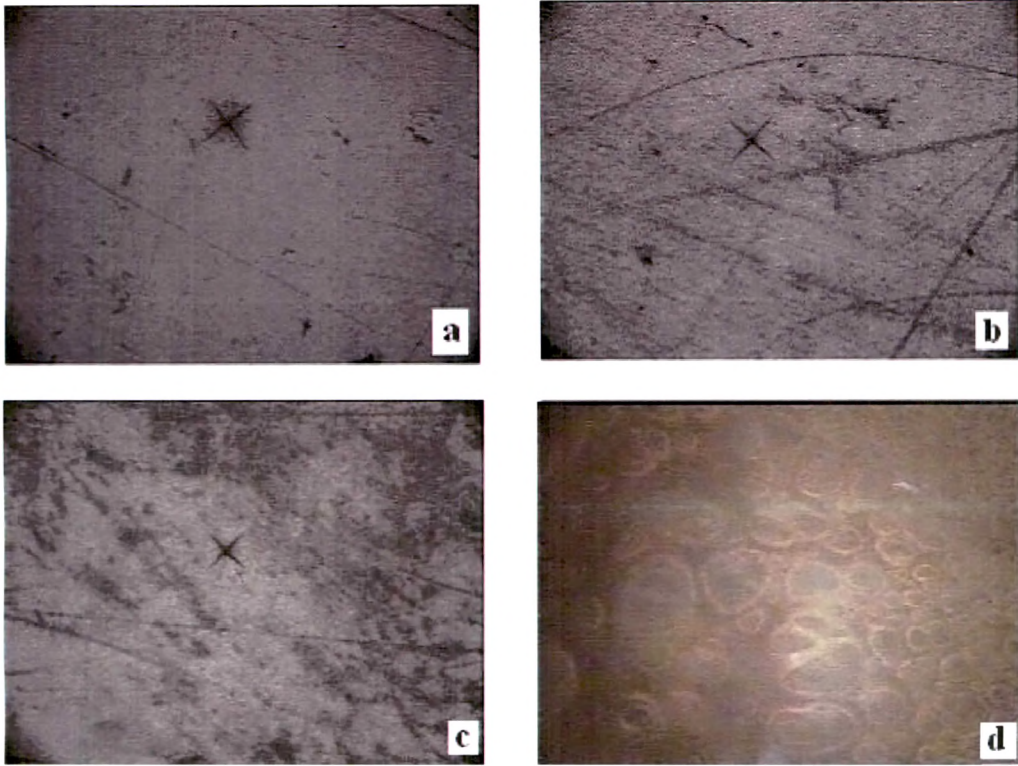


Figure 4.24: Optical micrographs for pristine and irradiated polyethylene terephthalate films (a) Pristine, (b)  $10^{13}$  ions/cm<sup>2</sup>, (c)  $10^{14}$  ions/cm<sup>2</sup> and (d)  $10^{15}$  ions/cm<sup>2</sup>.

#### 4.4 Polyether sulfone

Polyether sulfone (PES) plays an ever increasing role in microelectronics and aerospace applications due to its attractive dielectric, mechanical, thermal and chemical properties. It acts a like polycarbonate, but PES is a more heat resistant. It can also stand up well to water and steam, so it is used to make things like cookware and medical products that need to be sterilized between uses. Its chemical resistance is not as wide as PEEK's; hence stable solutions can be made if solvents are correctly chosen.

Only a few papers have mentioned the effects of low and high energy ions on PES. Wang et al [28] studied the dose rate effects on the electrical properties of several polymers (PES, PEEK, PS and PSA) implanted by 50 keV atomic and molecular nitrogen ions. They have reported that the electrical conductivity of these polymers shows significant changes with varying dose rate. These changes could not be explained by target temperature effects. The current-voltage characteristics and the temperature dependence of resistivity were also found to be influenced by varying the dose rate. Bridwell et al [29] studied the effects of 50 keV ions of He, B, C, N, Ar and As on PET, PAN, PES and PEEK polymers. The surface resistivity versus dose in the range  $10^{16}$ - $10^{17}$  ions/cm<sup>2</sup> indicates a plateau effect that are dependent on the incident ion and the target polymer. They have also reported that aliphatic or partially aliphatic polymers such as PET and PAN will reach lower resistivity than polymers that have more fully aromatic structures such as PEEK and PES. Evelyn et al [30] irradiated the stack of thin films of PES, PS and PVC by 5 MeV helium ions and studied the radiation induced changes in chemical structure of polymers. The

presence of sulfone and phenyl groups in the chemical composition of PES results in heat resistance and stability of the polymer to ionizing radiation.

Pristine and irradiated PES films were characterized through structural (FTIR spectroscopy), electrical (an LCR meter), thermal (TGA and DSC), mechanical (microhardness tester) and surface morphology [31,17].

#### 4.4.1 Structural Analysis

**Figure 4.25** shows the spectra of pristine and irradiated PES samples. The absorption bands as obtained from the pristine spectrum are identified as (A)  $720\text{ cm}^{-1}$ :  $\text{CH}_2$  absorption bands; (B)  $890\text{ cm}^{-1}$ : C-H bending vibration; (C)  $1080\text{ cm}^{-1}$ : C=S stretching vibration; (D)  $1730\text{ cm}^{-1}$ : C=O stretching vibration; (E)  $1950\text{ cm}^{-1}$ : C=C stretching vibration; (F)  $3000\text{ cm}^{-1}$ : C-H stretching vibration. It is observed that there is no change in overall structure of the polymer but a minor change in intensities have been observed up to the fluence of  $10^{14}\text{ ions/cm}^2$ . It may be concluded that PES is resistant to radiation at least up to the fluence of  $10^{14}\text{ ions/cm}^2$ . The spectrum corresponding to the fluence of  $10^{15}\text{ ions/cm}^2$  indicates a very significant change in the structure of polymer. This might be due to the breakage of bonds in the structure as well as formation of unsaturated structure. Further at this fluence, there was severe surface roughening (as observed through optical microscope **Figure. 4.32**) and because of severe roughness there is drastic fall in transmitted intensity due to scattering of IR from the surface.

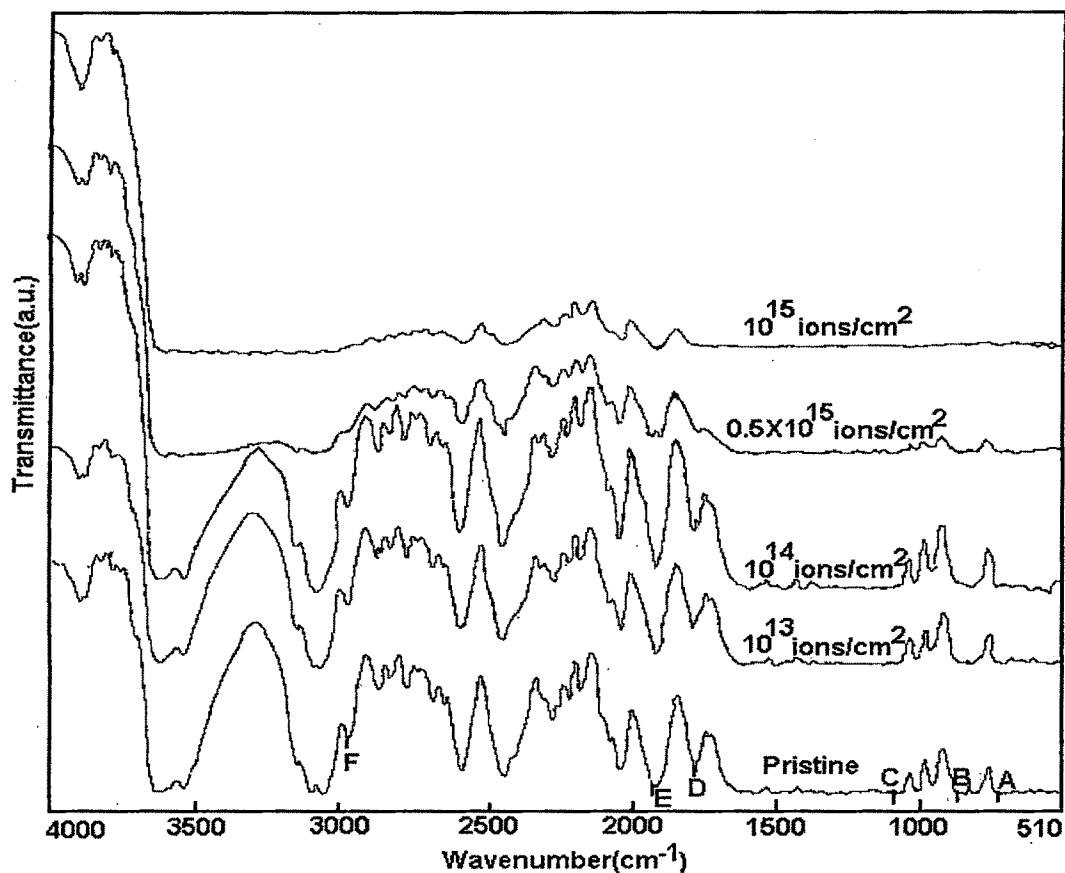


Figure 4.25: FTIR spectra for pristine and irradiated polyether sulfone films.

#### 4.4.2 Electrical Property

Electrical properties of pristine and irradiated samples were studied using an LCR meter in the frequency range 100 Hz-1MHz. The resistance, capacitance and dielectric loss measurements were carried out at ambient temperature. AC conductivity was calculated using equation 2.17 and dielectric constant by equation 2.19 as discussed in Chapter 2.

- **AC electrical frequency response**

AC conductivity measurement was performed for irradiated and pristine PES samples as shown in **Figure 4.26**. A sharp increase in conductivity has been observed around 300 kHz for pristine and irradiated samples. It is also observed that conductivity increases as fluences increases. The increase in conductivity due to irradiation may be attributed to scissioning of polymer chains and as a result increase of free radicals, unsaturation etc. An ac field of sufficiently high frequency applied to metal polymer metal structure may cause a net polarization, which is out of phase with the field. This results in ac conductivity, it appears at frequency greater than that at which traps are filled or emptied [6].

**Figure 4.27** shows a plot of  $\tan \delta$  versus log frequency for pristine and irradiated PES films. It is observed that  $\tan \delta$  is higher for irradiated sample and shows dominance of inductive behavior.

As evident from the graph (**Figure 4.28**) the dielectric constant remains almost constant up to 100 kHz and then decreases at higher frequencies. At the lower frequency, the mobility of free charge carriers is constant and so dielectric constant is constant. As the frequencies increases the charge carriers migrate through the dielectric and get trapped against a defect sites and induce an opposite charge in its vicinity, as a result of which they slow down and the value of dielectric constant decreases.

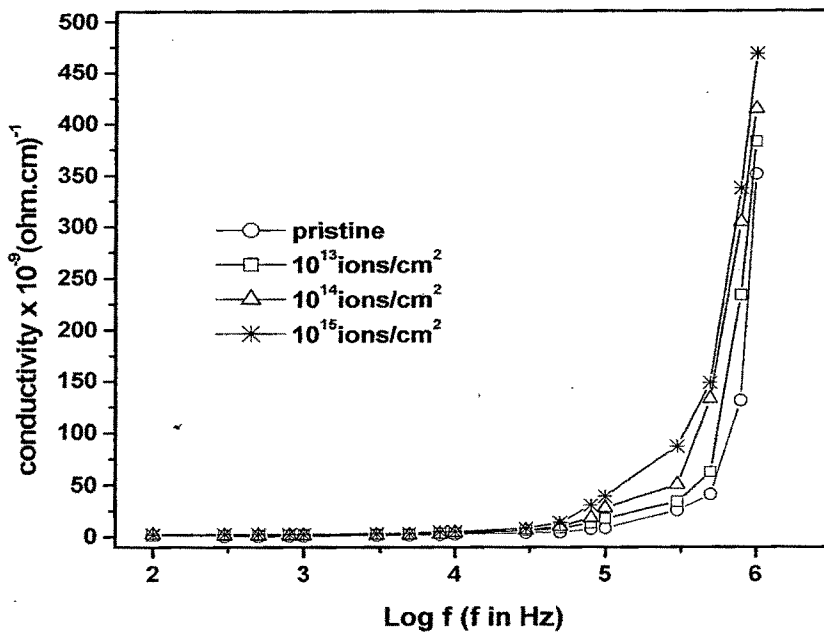


Figure 4.26: Conductivity versus Log f for pristine and irradiated polyether sulfone films.

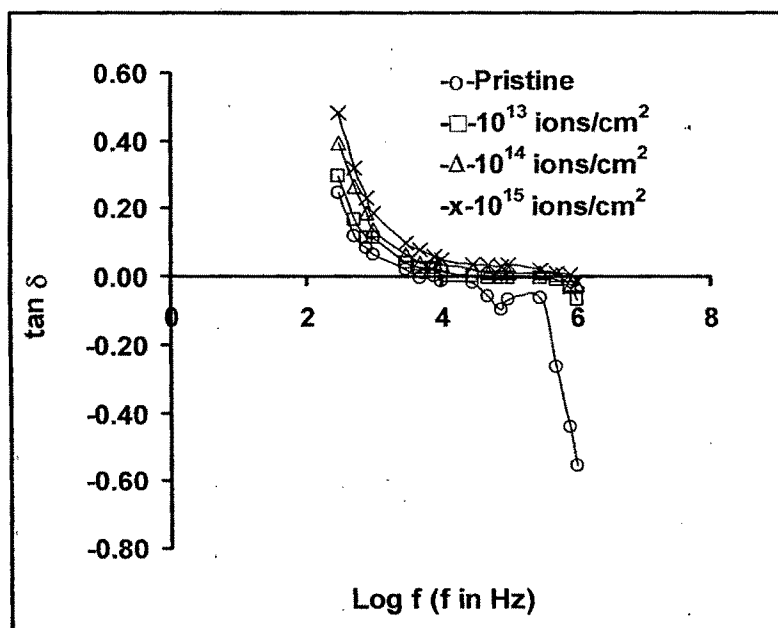


Figure 4.27:  $\tan \delta$  versus Log f for pristine and irradiated polyether sulfone films.

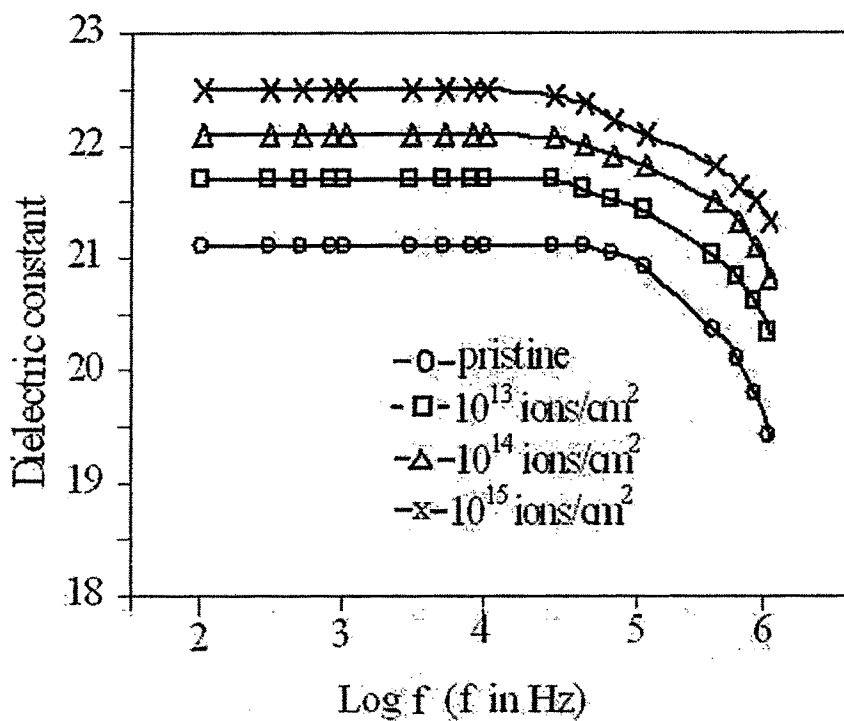


Figure 4.28: Dielectric constant versus Log f for pristine and irradiated polyether sulfone films.

#### 4.4.3 Thermal Studies

Thermogravimetric analysis and differential scanning calorimetry measurements were done to study the thermal response of pristine and irradiated samples.

##### 4.4.3.1 TGA analysis

TGA thermograms of pristine and irradiated PES are shown in Figure 4.29. The thermal stability was found to decrease with the increase of fluence. The pristine PES was stable up to the temperature of 410°C while irradiated sample is stable up to the temperature of 150°C with no loss of weight. The stable zone is followed by slow decomposition rate. Due to limited heating

temperature of 500°C, the weight loss of pristine and irradiated ( $10^{15}$  ions/cm<sup>2</sup>) PES up to this temperature was observed to be about 5% and 10% respectively. The decrease in thermal stability was observed at higher fluence ( $10^{15}$  ions/cm<sup>2</sup>), which implies that chain scission proceeds preferentially compared with cross linking.

#### **4.4.3.2 DSC analysis**

**Figure 4.30** shows the DSC thermograms of pristine and irradiated PES samples.  $T_g$  was observed at 225°C in pristine sample, and was also present in the irradiated ( $10^{14}$  ions/cm<sup>2</sup>) sample. Due to limited heating temperature,  $T_m$  was not observed in both the samples.

#### **4.4.4 Mechanical Property (microhardness)**

We have studied the mechanical property (microhardness) by means of Vickers' microhardness tester. The Vickers' hardness was calculated using equation 2.4 as discussed in Chapter 2.

**Figure 4.31** show the plot of Vickers' microhardness (Hv) versus applied load (P) for pristine and irradiated films. It is evident that the Hv value increases with the load up to 200 mN and then saturates beyond the load of 400 mN. The increase of Hv with load can be explained on the basis of the strain-hardening phenomenon. On applying the load, the polymer is subjected to some strain hardening and beyond certain loads the polymer exhausts its strain hardening capacity and the hardness tends to become constant. The rate of strain hardening is greater at low loads and decreases at higher loads.

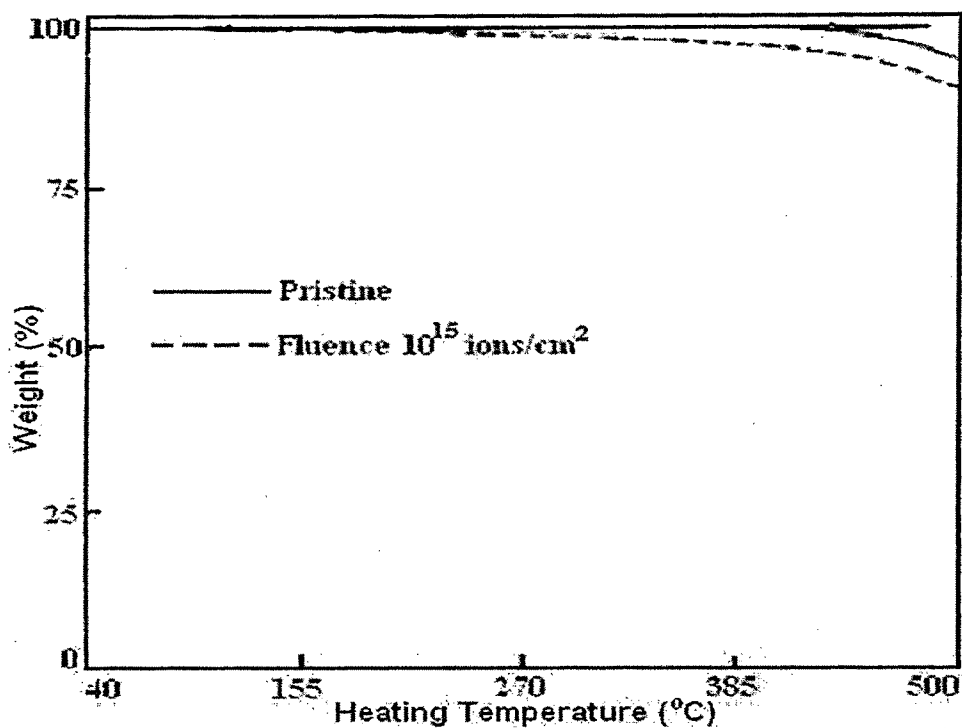


Figure 4.29: TGA thermograms for pristine and irradiated polyether sulfone films.

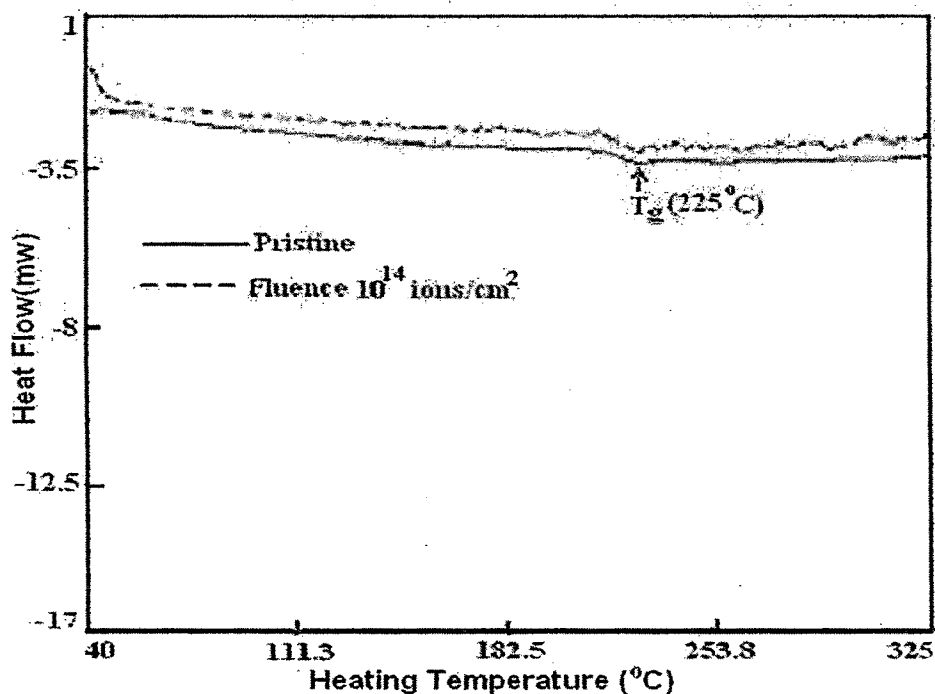


Figure 4.30: DSC thermograms for pristine and irradiated polyether sulfone films.

As can be seen that the hardness becomes independent of loads for load more than 400mN. The value obtained from the saturation region, therefore, represents the true hardness of the bulk materials. Since at high loads the indenter penetration depth is also high and surface effects become insignificant. It is also observed that the hardness increases as fluence increases. This may be attributed to the cross-linking phenomenon [18]. However, on further increase of the fluence, the polymer degrades its mechanical strength and as a result the hardness decreases at the fluence of  $10^{15}$  ions/cm<sup>2</sup>. The degradation may be a result of scissioning of the chemical bonds at the higher fluences. It is also observed from the FTIR spectra (**Figure 4.25**) that the structure of the polymer changed at the fluence of  $10^{15}$  ions/cm<sup>2</sup>.

#### **4.4.5 Surface Morphology**

Polyether sulfone is pale amber in colour. After modification with proton beam, no change in colour observed for  $10^{13}$  ions/cm<sup>2</sup>, but further increase of the fluence the irradiated samples became light-yellow and dark brown at the fluence of  $10^{14}$  and  $10^{15}$  ions/cm<sup>2</sup> respectively. **Figure 4.32** shows the optical micrographs of pristine and irradiated PES samples. When these polymers were observed through optical microscope, the irradiated samples do not appear to be flat (smooth), but seem to be rough. The roughness of the sample increases as fluence increases.

#### **4.4.5 Conclusion**

The FTIR spectra revealed that PES get chemically degraded at the

fluence of  $10^{15}$  ions/cm<sup>2</sup>. There is an exponential increase in conductivity with log frequency and the effect is significant at higher fluences. The value of dielectric constant and loss factor increases with the fluence. The decrease in thermal stability at the highest fluence indicates that the polymer underwent chain scission by proton irradiation and as a results, an increase of free radicals etc. It is noted from the optical micrographs that the irradiated samples do not appear to be flat (smooth). It became rough and the roughness of polymer increases as the fluence increases. The Vickers' microhardness of the polymer increases up to the fluence of  $10^{14}$  ions/cm<sup>2</sup>, probably due to cross-linking without any degradation effect. However, the hardness decreases at the fluence of  $10^{15}$  ions/cm<sup>2</sup> because of degradation of polymer due to scissioning of bonds, which is also corroborated by the FTIR spectra.

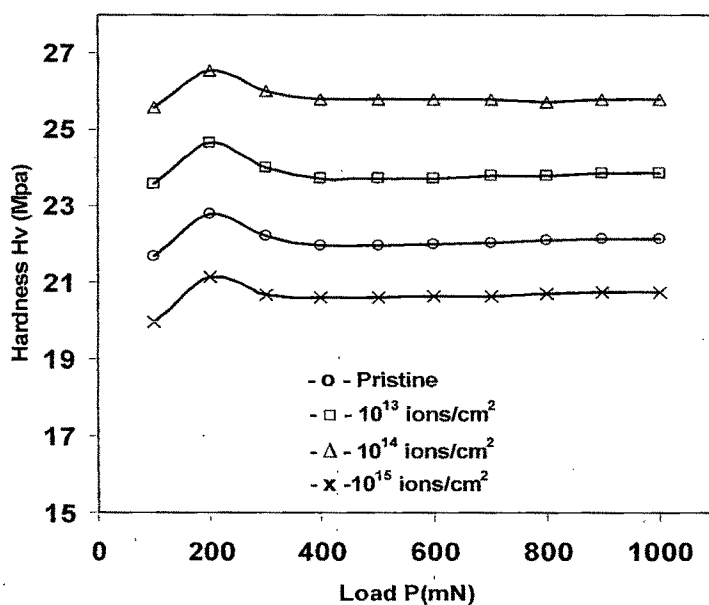


**Figure 4.31: Microhardness for pristine and irradiated polyether sulfone films.**

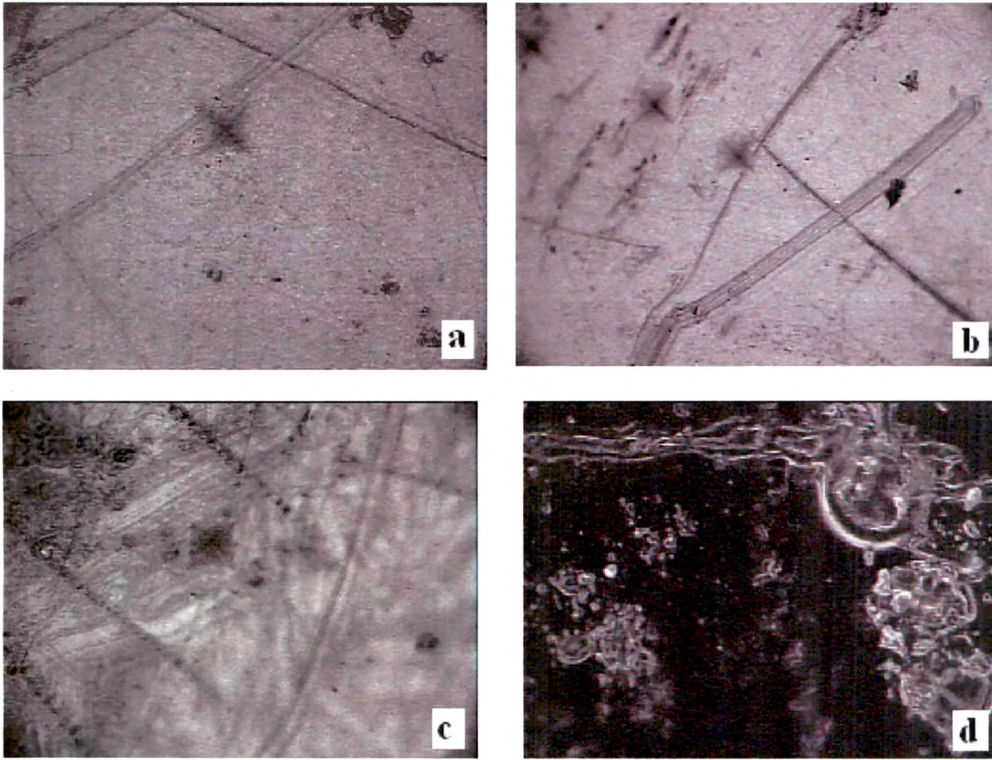


**Figure 4.32: Optical micrographs of pristine and irradiated polyether sulfone films (a) pristine, (b)  $10^{13}$  ions/cm<sup>2</sup>, (c)  $10^{14}$  ions/cm<sup>2</sup> and (d)  $10^{15}$  ions/cm<sup>2</sup>.**

#### 4.5 Polycarbonate/Makrofol-DE

Polycarbonate (makrofol-DE) is an amorphous polymer with attractive engineering properties including high impact strength, low moisture absorption, low combustibility, good dimensional stability and high light transmittance. The latter property has resulted in the application of PC as an impact-resistance substitute for window glass. Applications include glazing, safety shields, lenses, eyeglasses, casings and housings, light fittings, kitchenware (microwaveable), medical apparatus (sterilisable) and CD's (the discs).

The effect of ion beam irradiation on PC has already been reported. Ferain and Legras [32] reported the chemical modifications induced by swift heavy ions (SHI) on a model compound of PC, i.e. diphenyl carbonate (DPC). They have established the similarity between heavy ion irradiation and heat treatment. On the basis of these results, they explained the preferential chemical attack along the tracks of the irradiated film. Steckenreiter et al [33] studied the degradation processes in PC induced by SHI irradiations inducing electronic stopping power higher than  $4.0 \text{ MeV mg}^{-1}\text{cm}^2$ . They observed alkyne formation in all irradiated samples using insitu Fourier transform infrared (FTIR) spectroscopy. Mishra et al [15] studied the thermal and structural properties of 62 MeV protons irradiated PC at different doses (10, 30, 60 and 80 kGy). They have reported no prominent variation in the absorbance bands of MFN and observed modification in thermal properties of MFN, which is dose dependent. Thermal analysis is further corroborated the fact that chain-scission is the dominant phenomena in irradiated MFN samples resulting in the reduction of its thermal stability by about 19%. Piraux et al [34] studied PC particle track-etched

membranes used as templates in nano-tubes and nano-wires manufacturing. Dehaye et al [35] studied the chemical modifications in bisphenol A polycarbonate induced by swift heavy ion irradiations and analyzed in situ by means of FTIR spectroscopy. Four beams ( $^{13}\text{C}$ ,  $^{20}\text{Ne}$ ,  $^{48}\text{Ca}$ ,  $^{129}\text{Xe}$ ) with energy of a few MeV/amu have been used. The FTIR spectra obtained after the irradiation exhibit an overall reduction in the intensities of the virgin PC typical vibration bands and the appearance of new bands. The analysis of the destruction and the new vibration bands points out that the energy deposition mechanisms are quite different depending on electronic stopping power. Wang et al [36] and Zhu et al [37] reported chemical changes in PC induced by very high energetic ions (>GeV) by using ex-situ FTIR spectroscopy. They also studied alkyne creation in irradiated PC for electronic stopping power values higher than  $3.3 \text{ MeV mg}^{-1} \text{ cm}^2$ . Chipara and Reyes-Romero [38] reported electron spin resonance (ESR) investigations of SHI irradiated PC performed to study the nature of free radicals as well as exchange interactions among them on the basis of track structure.

In the present work, Polycarbonate was irradiated with 3 MeV proton beam at different fluences. Pristine and irradiated PC (MFD) films were characterized through structural (FTIR spectroscopy), electrical (LCR meter), thermal (TGA and DSC), mechanical (microhardness tester) and surface morphology [39].

#### 4.5.1 Structural Analysis

The FTIR spectra of the pristine and irradiated samples are shown in **Figure 4.33**. The absorption bands as obtained from the pristine spectrum are identified as: (A)  $765 \text{ cm}^{-1}$ : out of phase skeletal vibration of C-H deformation;

(B)  $1030\text{ cm}^{-1}$ : C-O stretching vibration; (C)  $1645\text{ cm}^{-1}$ : C=C phenyl ring stretching vibration; (D)  $1775\text{ cm}^{-1}$ : C=O stretching vibration; (E)  $2594\text{ cm}^{-1}$ : hydroxyl stretching bond; (F)  $2968\text{ cm}^{-1}$ :  $\text{CH}_3$  stretching vibration; (G)  $3060\text{ cm}^{-1}$ : C-H stretching vibration of aromatic compounds. It is observed that there is no change in overall structure of the polymer but minor changes in intensities were observed up to the fluence of  $10^{14}\text{ ions/cm}^2$ . The minor changes in the intensity of peaks of the irradiated samples may be due to the breakage of few bonds in the ladder structure, but this will not change the overall structure of the polymer. The spectrum corresponding to  $10^{15}\text{ ions/cm}^2$  revealed that the material suffered severe degradation through scissioning of polymer chains and as a result, significant change in the structure of the polymer.

#### 4.5.2 Electrical Property

Electrical properties of pristine and irradiated samples were studied using an LCR meter in the frequency range 100 Hz-1MHz. The resistance, capacitance and dielectric loss measurements were carried out at ambient temperature. AC conductivity was calculated using equation 2.17 and dielectric constant by equation 2.19 as discussed in Chapter 2.

- **AC Electrical Frequency Response**

Figure 4.34 shows the variation of electrical conductivity with log frequency for the pristine and irradiated samples. A sharp increase in conductivity was observed around 300 kHz for pristine and irradiated samples. It is also observed that the conductivity increases as fluence increases.

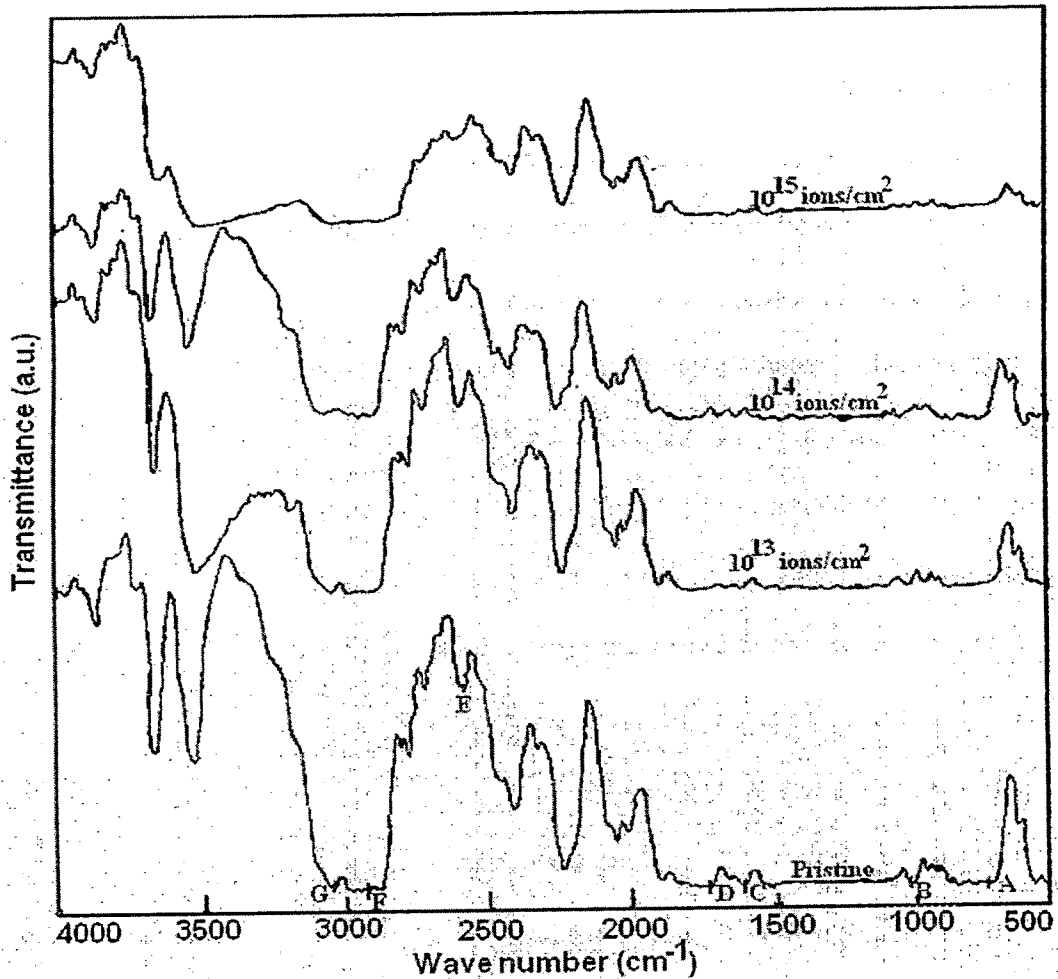


**Figure 4.33:** FTIR spectra for pristine and irradiated polycarbonate films.

The increase in conductivity due to irradiation may be attributed to scissioning of the polymer chains, resulting in an increase of free radicals, unsaturation, etc. An AC field of sufficiently high frequency applied to a metal-polymer-metal structure may cause a net polarization, which is out of phase with the field. This results in AC conductivity; it appears at frequencies greater than that at which traps are filled or emptied [6].

**Figure 4.35** represents a plot of loss factor ( $\tan \delta$ ) versus log frequency for pristine and irradiated polycarbonate (MFD) films at ambient temperature.

The loss factor ( $\tan \delta$ ) decreases exponentially as frequency increases. It is also observed that the loss factor increases as fluence increases. The increase in loss factor with fluence may be due to scissioning of polymer chains, resulting in an increase of free radicals etc. The  $\tan \delta$  has a positive value, indicating the dominance of inductive behavior.

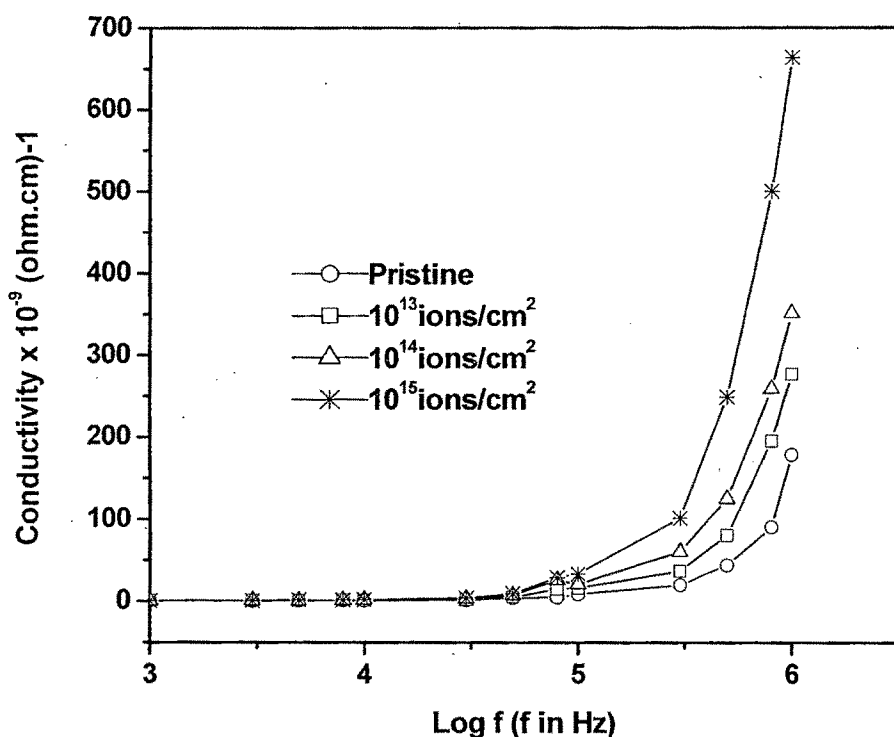


Figure 4.34: Conductivity versus Log f for pristine and irradiated polycarbonate films.

Figure 4.36 shows a plot of dielectric constant ( $\epsilon$ ) versus Log f at ambient temperature for pristine and irradiated polycarbonate samples. As evident from the graph, the dielectric constants remain almost constant up to 100 kHz and then decreases at higher frequencies. At lower frequencies the mobility of the free charge carriers is constant and thus the dielectric constant is constant. As

the frequency increases, the charge carriers migrate through the dielectric and get trapped against a defect sites and induce an opposite charge in its vicinity, as a result of which motion of charge carriers is slowed down and the value of dielectric constant decreases.

### **4.5.3 Thermal Studies**

The thermal response of pristine and irradiated MFD samples was studied by two techniques viz., (i) Thermogravimetric analysis and (ii) Differential scanning calorimetry.

#### **4.5.3.1 TGA analysis**

As depicted in **Figure 4.37**, the pristine and irradiated (at the fluence of  $10^{14}$  ions/cm<sup>2</sup>) samples are thermally stable up to 313 °C and 296 °C respectively. On the other hand, the stability of irradiated sample (at the fluence of  $10^{15}$  ions/cm<sup>2</sup>) only remained up to 255°C. This change clearly indicates that up to the fluence of  $10^{14}$  ions/cm<sup>2</sup>, the system remains reasonably organized but becomes quite disorganized when the fluence of  $10^{15}$  ions/cm<sup>2</sup> is used and thermal stability reduced by about 19%. At the limiting heating temperature of 500 °C, the weight loss of pristine and irradiated polycarbonate was about 46%, 48% and 59%, respectively. From the data, it is evident that no significant change was observed up to the fluence of  $10^{14}$  ions/cm<sup>2</sup>, which is also shown by FTIR spectroscopy (**Figure 4.33**).

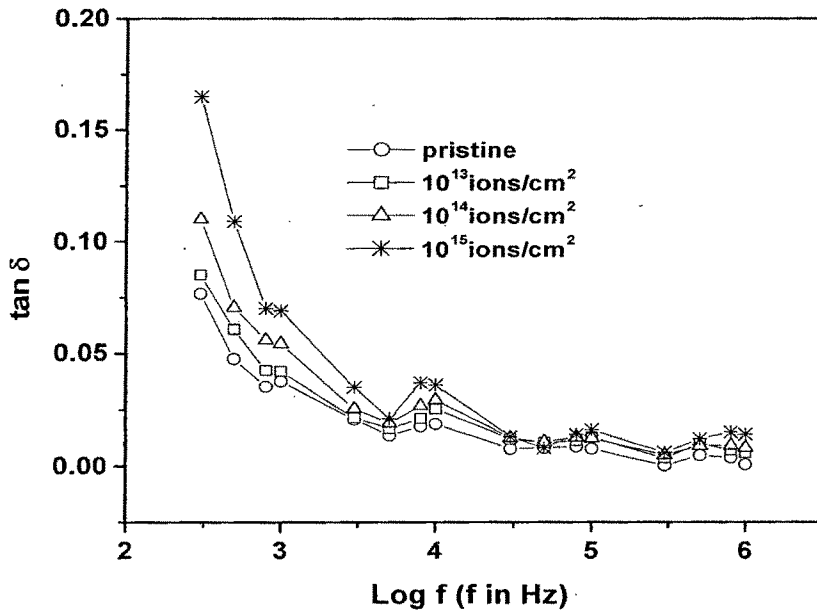


Figure 4.35:  $\tan \delta$  versus  $\text{Log } f$  for pristine and irradiated polycarbonate films.

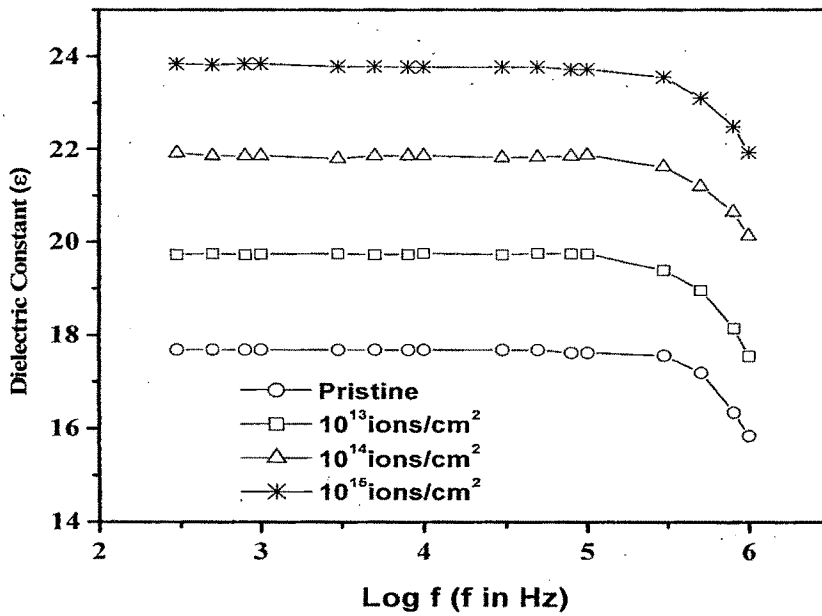


Figure 4.36: Dielectric constant versus  $\text{Log } f$  for pristine and irradiated polycarbonate films.

The activation energy for the polymer decomposition process was calculated from the TGA patterns using the eq<sup>n</sup>.  $\ln(\ln(m_0/m))=E/R(1/T)$ , where E is activation energy of decomposition,  $m_0$  is the initial mass, m is the mass at temperature T and R is the universal gas constant [9]. The plots of  $\ln(\ln(m_0/m))$  vs  $10^3/T$  ( $K^{-1}$ ) is shown in **Figure 4.38**. The activation energies are 136.87 kJ/mol and 95.56 kJ/mol for pristine and irradiated ( $10^{15}$  ions/cm<sup>2</sup>) PC respectively. This denotes a degradation of the polymer matrix under proton irradiation, making it to start decomposition earlier than the pristine PC.

#### **4.5.3.2 DSC analysis**

**Figure 4.39** shows the DSC thermograms for pristine and irradiated samples. The glass transition temperature ( $T_g$ ) appeared around 146°C and no melting endotherm ( $T_m$ ) peak was observed in the pristine sample. By increasing the ion fluence up to  $10^{14}$  ions/cm<sup>2</sup>, the  $T_g$  was shifted to lower temperature (i.e.144 °C). The minor change observed due to the cross-linking and scissioning of the irradiated polycarbonate, which is also corroborated from TGA thermogram and FTIR spectrum at the fluence of  $10^{14}$  ions/cm<sup>2</sup>. The decrease in  $T_g$  with further increase in proton fluence support the fact that chain scission predominates by irradiation.

#### **4.5.4 Mechanical Property (microhardness)**

We have studied the mechanical property (microhardness) by means of Vickers' microhadness tester. The Vickers' hardness was calculated using equation 2.4 as discussed in Chapter 2.

Figure 4.40 show the plot of Vickers' microhardness (Hv) versus applied load (P) for pristine and irradiated PC films. It is evident that the Hv value increases with the load up to 200mN and then saturates beyond the load of 400 mN.

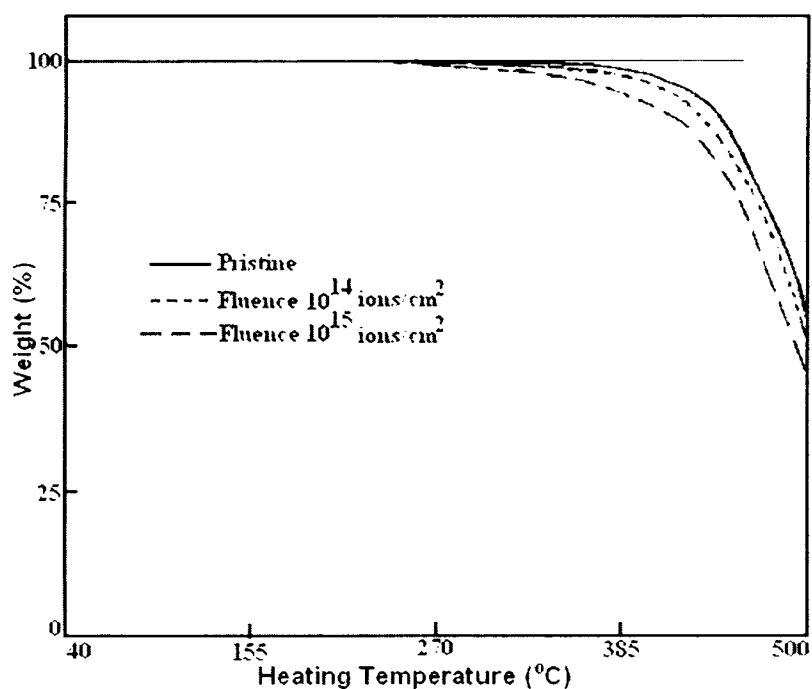


Figure 4.37: TGA thermograms for pristine and irradiated polycarbonate films.

The increase of Hv with load can be explained on the basis of the strain-hardening phenomenon. On applying the load, the polymer is subjected to some strain hardening and beyond certain loads the polymer exhausts its strain hardening capacity and the hardness tends to become constant. The rate of strain hardening is greater at low loads and decreases at higher loads.

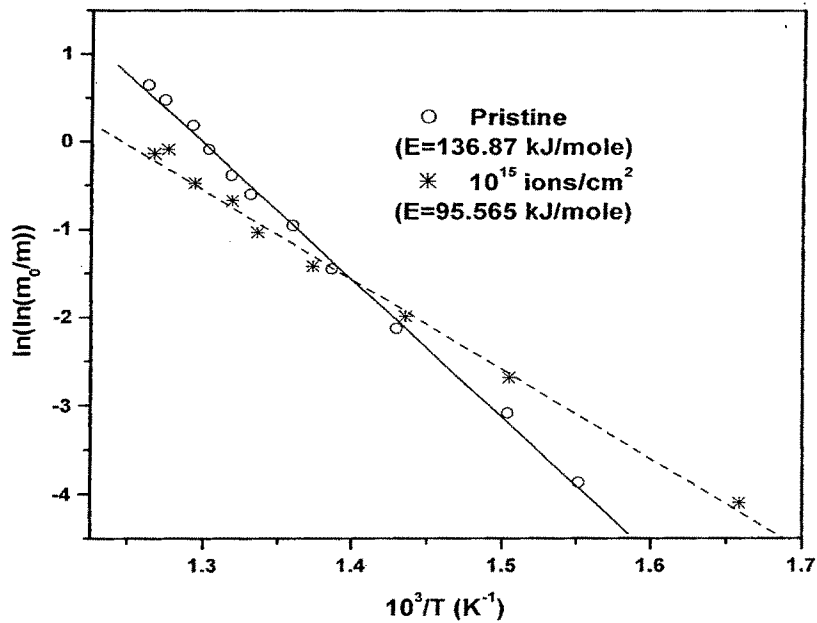


Figure 4.38:  $\ln(\ln(m_0/m))$  versus  $10^3/T$  ( $K^{-1}$ ) for the pristine and irradiated polycarbonate films.

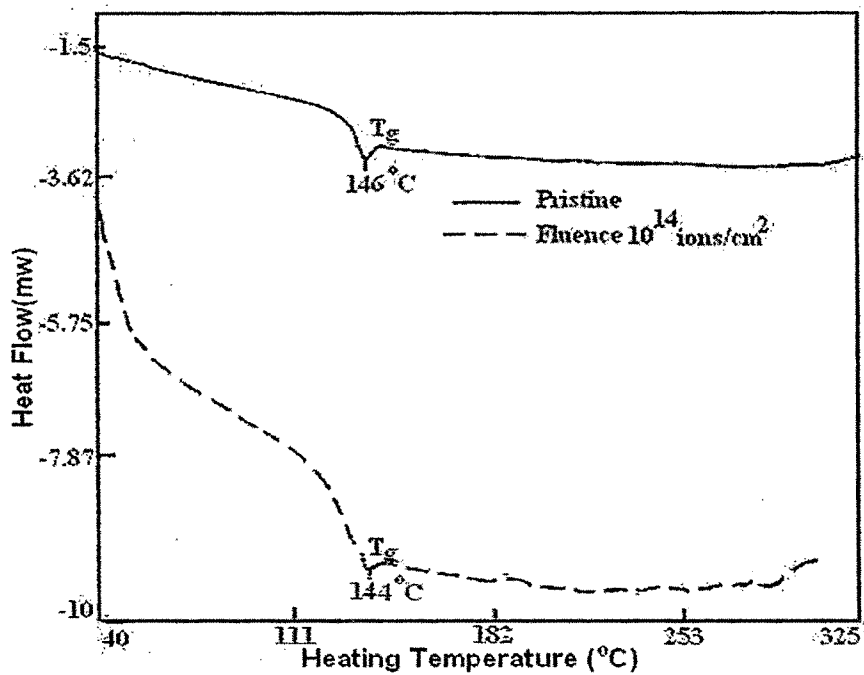


Figure 4.39: DSC thermograms for pristine and irradiated polycarbonate films.

As can be seen that the hardness becomes independent of loads for load more than 400mN. The value obtained from the saturation region, therefore, represents the true hardness of the bulk materials. Since at high loads the indenter penetration depth is also high and surface effects become insignificant. It is also observed that the hardness increases as fluence increases. This may be attributed to the cross-linking phenomenon [18]. At the fluence of  $10^{15}$  ions/cm<sup>2</sup>, the surface become dark brown and Microhardness indentation mark could not be observed on the surface.

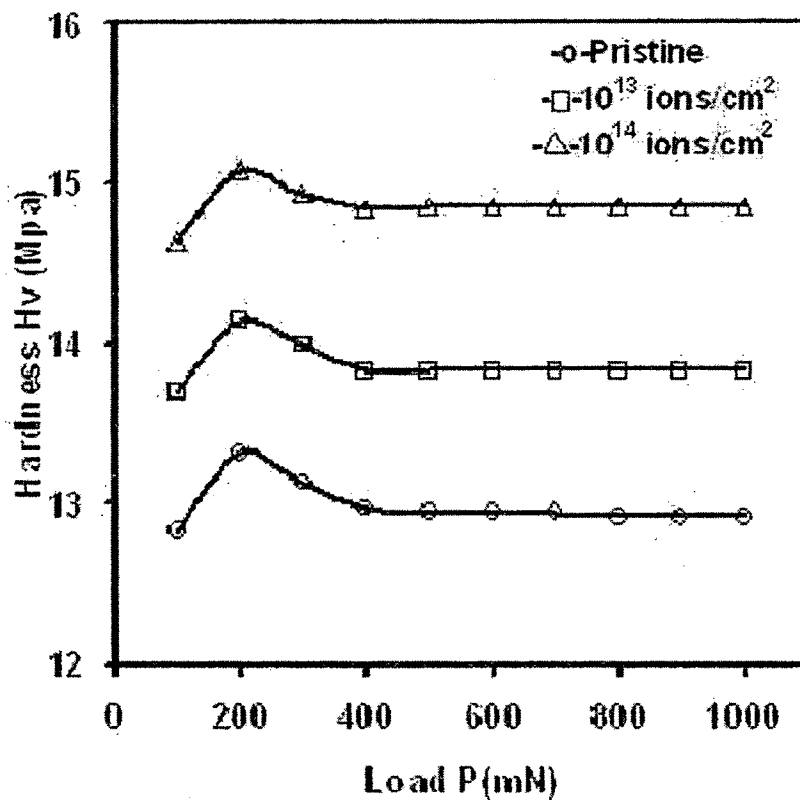


Figure 4.40: Microhardness for pristine and irradiated polycarbonate films.

#### 4.5.5 Surface Morphology

The modification in surface morphology are found with the change in colour of the polymers, which is transparent for pristine film and no appreciable change in colour has been observed at the fluence of  $10^{13}$  ions/cm<sup>2</sup>. On further increase of the fluence the surface became slight yellow and dark brown for irradiated samples at the fluence of  $10^{14}$  ions/cm<sup>2</sup> and  $10^{15}$  ions/cm<sup>2</sup> respectively. **Figure 4.41** shows the optical micrographs of PC samples. It is observed that surface become rough and roughness increases as fluences increase.

#### 4.5.6 Conclusion

The FTIR spectra indicate that MFD is chemically degraded at the highest proton fluence used, viz.  $10^{15}$  ions/cm<sup>2</sup>. On the other hand there was no significant change in the absorbance bands of MFD observed by proton irradiation up to the fluence of  $10^{14}$  ions/cm<sup>2</sup>. The minor changes in the peak's intensity of irradiated samples may be due to breakage of a few bonds in the ladder structure, but this will not change the overall structure of the polymer. The increase in dielectric properties due to irradiation may be attributed to scissioning of polymer chains, resulting in an increase of free radicals, unsaturation etc. The decrease in thermal stability at the highest proton fluence ( $10^{15}$  ions/cm<sup>2</sup>) indicates that the polymer underwent chain-scission by proton irradiation. No significant change in the position of  $T_g$  was observed for pristine and irradiated samples at the fluence of  $10^{14}$  ions/cm<sup>2</sup>, which is also

corroborated with TGA thermogram and FTIR spectra at the fluence of  $10^{14}$  ions/cm<sup>2</sup>. The Vickers' hardness of the PC sample increases up to a fluence of  $10^{14}$  ions/cm<sup>2</sup>, probably due to cross linking without any degradation effect. It is observed from the optical micrographs; that the irradiated samples do not appear to be flat (smooth). It became rough and the roughness of polymer surface increases as the fluence increases...

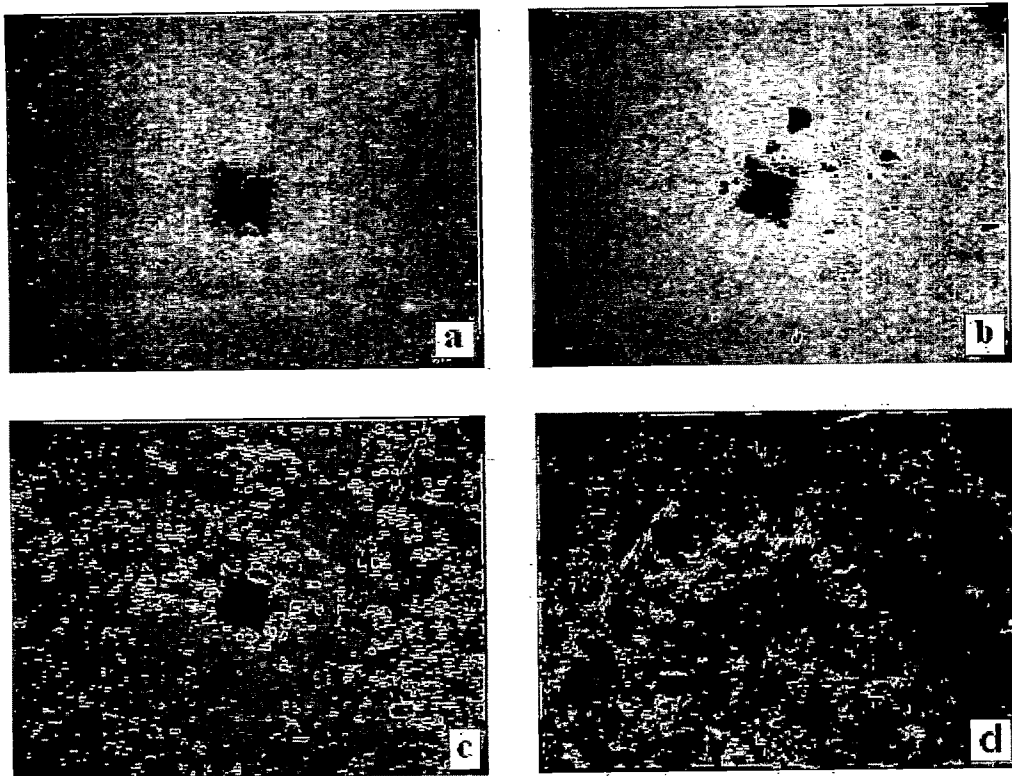


**Figure 4.41: Optical micrographs of pristine and irradiated polycarbonate films (a) Pristine, (b)  $10^{13}$  ions/cm<sup>2</sup>, (c)  $10^{14}$  ions/cm<sup>2</sup> and (d)  $10^{15}$  ions/cm<sup>2</sup>.**

## 4.6 Blend Polymer (PVC+PET)

The significant advantages of polymer blends are that the properties of the finished product can be tailored to the requirements of the applications, which can not be achieved alone by one polymer. PVC is an important material in cable insulation and sheathing; there is a much greater emphasis today on the use of non-halogenated materials in electrical insulation. An extremely important factor in the selection of insulation and sheathing materials is the flammability, smoke evolution and toxicity of the evolved gases. Since PVC has very good electrical properties whereas PET was chosen because of its very good mechanical strength due to the presence of the aromatic ring in polymer structure. This polymer was prepared in the laboratory in equal proportion of PVC with commercial grade PET in two roll mill as discussed in chapter 3.3.1. Four films were irradiated by 3MeV proton beam at different fluences of  $10^{13}$ ,  $0.5 \times 10^{14}$ ,  $10^{14}$  and  $10^{15}$  ions/cm<sup>2</sup> [40]. The unirradiated (pristine) and irradiated samples were characterized for structural, electrical (dielectric properties), thermal, mechanical (microhardness) properties and surface morphology as discussed in Chapter 2 (article 2.3).

### 4.6.1 Structural Analysis

The FTIR spectra of the pristine and irradiated samples are shown in **Figure 4.42**. The absorption bands as obtained from the pristine spectrum are identified as : (A)  $800 \text{ cm}^{-1}$ : C-Cl stretching vibration; (B)  $1485 \text{ cm}^{-1}$ : C-H Bending vibration; (C)  $1730 \text{ cm}^{-1}$ : C=O stretching vibration; (D)  $1950 \text{ cm}^{-1}$ : C=C stretching

vibration; (E)  $2335\text{cm}^{-1}$ :vibration of  $\text{CO}_2$ ; (F)  $2700\text{cm}^{-1}$ : O-H stretching vibration; (G)  $2850\text{cm}^{-1}$ : C-H stretching vibration.

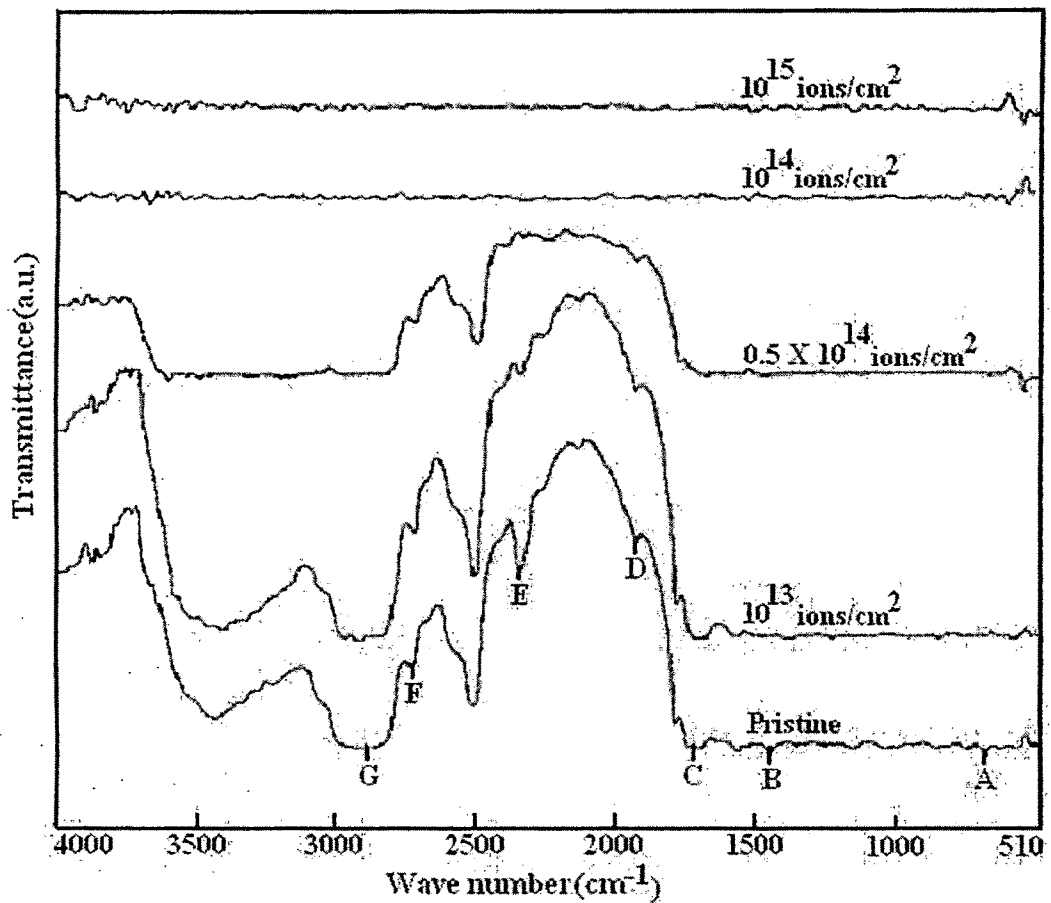


**Figure 4.42: FTIR spectra for pristine and irradiated blend polymer films.**

It is observed that there is no significant change in the intensities up to the fluence of  $10^{13}$  ions/ $\text{cm}^2$ . It is found that the absorption bands characteristic of all above functional groups declines, conforming their destruction by irradiation. These functional groups vanish gradually as irradiation proceeds. This may be attributed to scissioning of polymeric chains and the formation/emission of low molecule gases and radicals due to irradiation [22]. Further, the drastic changes in intensities of absorbance bands at the fluences of  $10^{14}$  ions/ $\text{cm}^2$ , and above, indicate that transmittance of IR beam from surface

decreases due to roughness/opaque. It may be speculated that scattering from the surface could also be a contributing factor in reducing the intensities of the absorbance/transmittance bands.

#### 4.6.2 Electrical Property

The electrical properties of pristine and irradiated samples were studied using an LCR meter. The resistance, capacitance and dielectric measurements were carried out over the frequency range 100 Hz-100 kHz at room temperature. AC conductivity was calculated using equation 2.17 and dielectric constant by equation 2.19 as discussed in Chapter 2.

- **AC electrical frequency response**

AC conductivity measurement was performed for irradiated and pristine samples as shown in **Figure 4.43**. A sharp increase in conductivity at 20 kHz has been observed in pristine as well as irradiated samples. It is also observed that the conductivity increases as fluence increases. The increase in conductivity due to irradiation may be attributed to scissioning of the polymer chains and as a result, an increase of free radicals, unsaturation, etc. An AC field of sufficiently high frequency applied to a metal-polymer-metal structure may cause a net polarization, which is out of phase with the field. This results in AC conductivity; it appears at frequencies greater than that at which traps are filled or emptied [6].

**Figure 4.44** shows variation of  $\tan \delta$  with log frequency for pristine and irradiated samples. It reveals that  $\tan \delta$  drops as frequency increases. It is also

observed that loss factor ( $\tan \delta$ ) increases as fluence increases.  $\tan \delta$  has positive values indicating the dominance of inductive behavior.

**Figure 4.45** shows the variation of dielectric constant with log frequency for the pristine and irradiated samples. It is seen that the dielectric constant remains almost unchanged over a wide frequency range and increases as fluence increases. This indicates that mobility of the free charge carriers is constant at these frequencies and so the dielectric constant does not change.

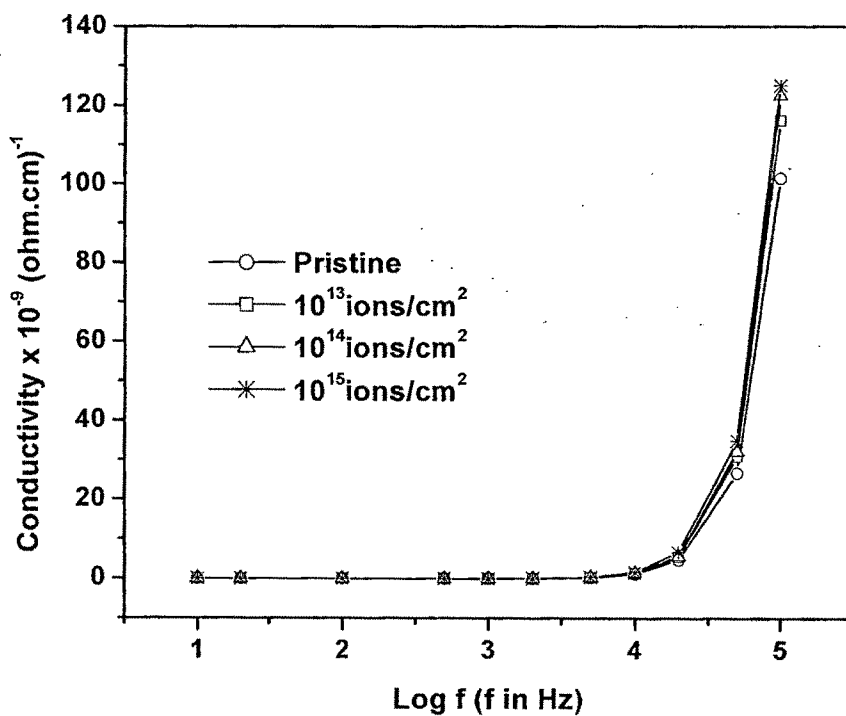


**Figure 4.43:** Conductivity versus Log f for pristine and irradiated blend polymer films.

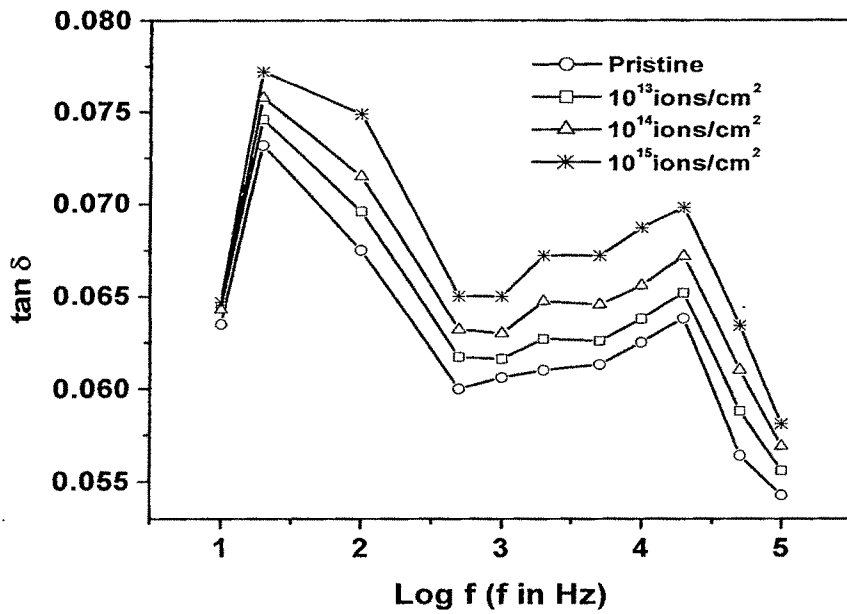


Figure 4.44:  $\tan \delta$  versus  $\text{Log } f$  for pristine and irradiated blend polymer films.

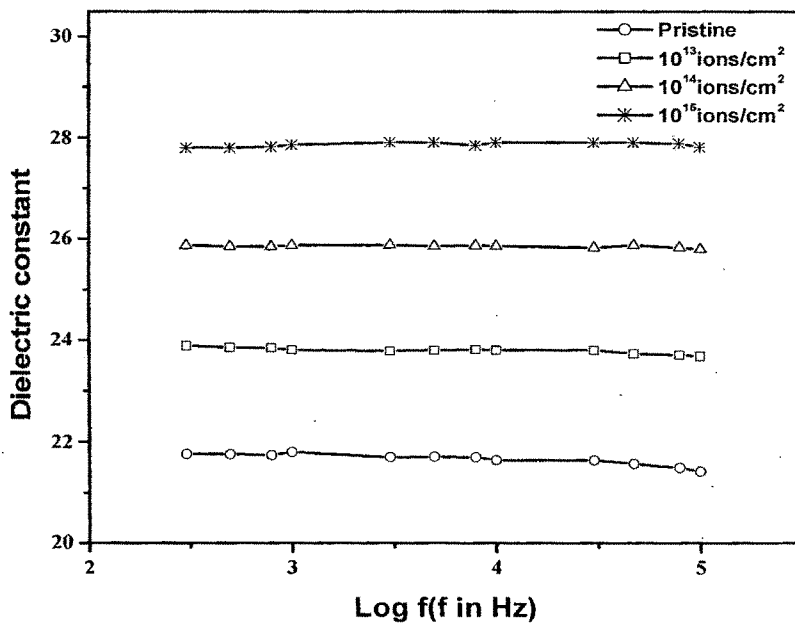


Figure 4.45: Dielectric constant versus  $\text{Log } f$  for pristine and irradiated blend polymer films.

### 4.6.3 Thermal Studies

Thermogravimetric analysis and differential scanning calorimetry were done to characterize the pristine and irradiated samples.

#### 4.6.3.1 TGA analysis

The decomposition behavior of the polymer was examined by TGA as shown in **Figure 4.46**. Thermogram shows two stage decomposition. As depicted from the figure, the stable zone disappeared for the irradiated ( $10^{15}$  ions/cm<sup>2</sup>) polymer, which was observed up to 169°C for pristine polymer. TGA thermograms indicate a degradation of the polymer matrix under proton irradiation making it to decompose earlier than the pristine sample, which is also corroborated by FTIR spectra (**Figure 4.42**).

The weight loss of about 10% and 25% has been observed for pristine and irradiated samples at the temperature of 270 °C, whereas a weight loss of about 72% and 70% has been observed for pristine and irradiated samples respectively at 500 °C. No appreciable change has been observed in the second stage.

The activation energy for the polymer decomposition process was calculated from the TGA patterns using the eq<sup>n</sup>.  $\ln(\ln(m_0/m)) = E/R(1/T)$ , where E is activation energy of decomposition,  $m_0$  is the initial mass, m is the mass at temperature T and R is the universal gas constant [9]. The plots of  $\ln(\ln(m_0/m))$  vs  $10^3/T$  (K<sup>-1</sup>) is shown for both stages in **Figure 4.47 (a) and (b)**. The activation energies for first stage are 95.81 kJ/mol and 12.926 kJ/mol for pristine and irradiated blend polymer respectively. The activation energies for second stage

are 11.22 kJ/mol and 36.13 kJ/mol for pristine and irradiated blend polymer respectively. As can be seen from thermograms (**Figure 4.46**), the weight loss of pristine sample is about 2% more than the irradiated one in the temperature range 285-500°C. This indicates that, in the second stage, the thermal stability of irradiated sample is better than the pristine one.

#### **4.6.3.2 DSC analysis**

**Figure 4.49** shows the DSC thermograms of pristine and irradiated ( $\sim 10^{13}$  and  $10^{14}$  ions/cm<sup>2</sup>) polymer films. The endotherm for the pristine film was observed at 249°C. By increasing the fluence the endotherm shifted to slightly higher temperature and then decreases to lower temperature on further increase of the fluence. This change clearly indicates that up to the fluences of  $10^{13}$  ions/cm<sup>2</sup>, the system remains reasonably organized but gets quite disorganized with some residual energy when fluence of  $10^{14}$  ions/cm<sup>2</sup> is used. From the analysis of DSC curves, it is observed that the endotherm consists of two peaks at the fluences of  $10^{14}$  ions/cm<sup>2</sup>, one at high and constant temperature related to the unchanged material and the other at low temperature related to damage material. This may be due to decrease in molecular weight [27].

#### **4.6.4 Mechanical Property (microhardness)**

We have studied the mechanical property (microhardness) by means of Vickers' microhardness tester. The Vickers' hardness was calculated using equation 2.4 as discussed in Chapter 2.

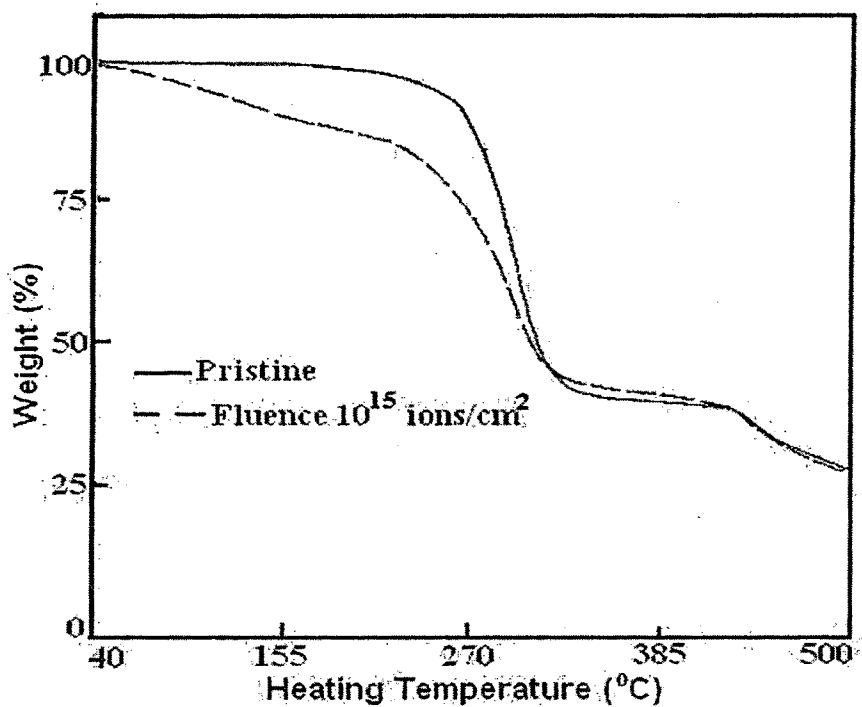


Figure 4.46: TGA thermograms for pristine and irradiated blend polymer films.

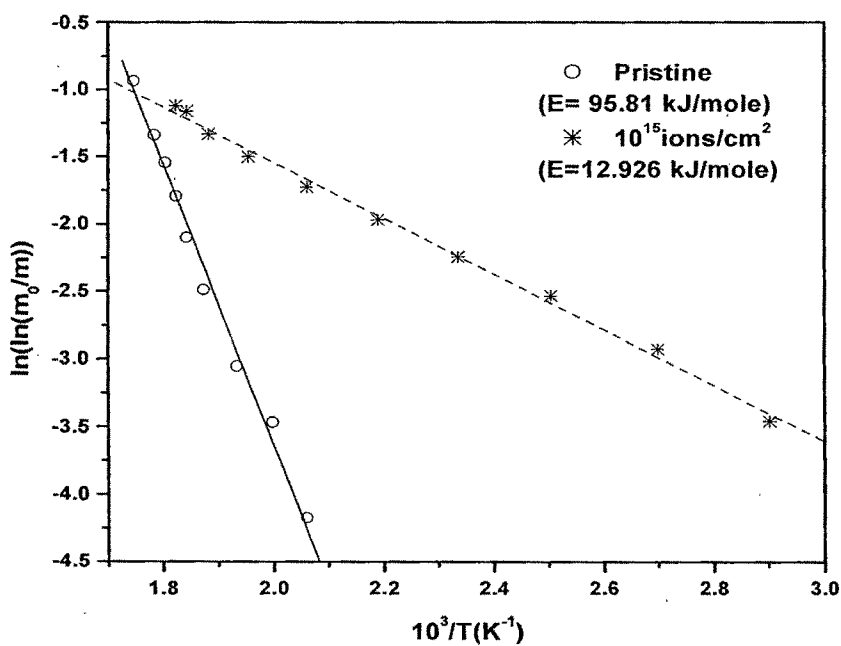


Figure 4.47(a):  $\ln(\ln(m_0/m))$  versus  $10^3/T$  ( $K^{-1}$ ) for the pristine and irradiated blend polymer films.

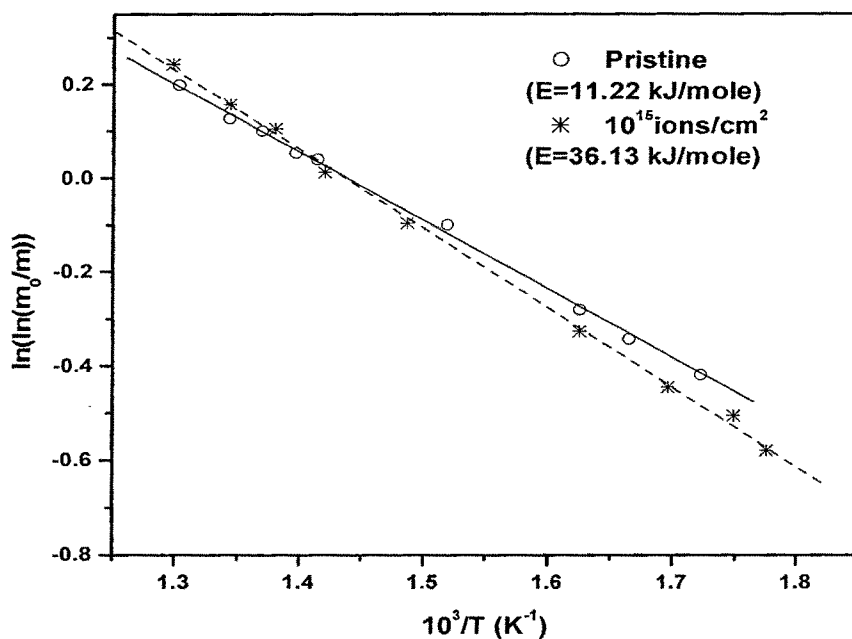


Figure 4.47(b):  $\ln(\ln(m_0/m))$  versus  $10^3/T$  (K<sup>-1</sup>) for the pristine and irradiated blend polymer films.

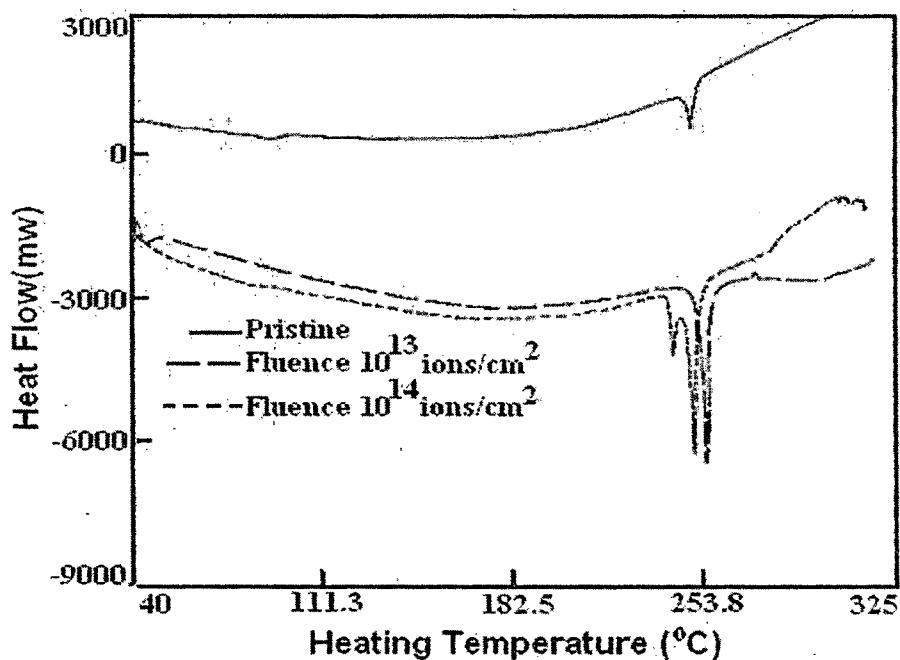


Figure 4.48: DSC thermograms for pristine and irradiated blend polymer films.

**Figure 4.50** show the plot of Vickers' microhardness (Hv) versus applied load (P) for pristine and irradiated films. It is evident that the Hv value increases with the load up to 200mN and then saturates beyond the load of 400 mN. The increase of Hv with load can be explained on the basis of the strain-hardening phenomenon. On applying the load, the polymer is subjected to some strain hardening and beyond certain loads the polymer exhausts its strain hardening capacity and the hardness tends to become constant. The rate of strain hardening is greater at low loads and decreases at higher loads [18].

As can be seen that the hardness becomes independent of loads for load more than 400 mN. The value obtained from the saturation region, therefore, represents the true hardness of the bulk materials. Since at high loads the indenter penetration depth is also high and surface effects become insignificant. It is also observed that the hardness increases as fluence increases. This may be attributed to the cross-linking phenomenon [18]. On further increase of fluence (i.e.  $10^{14}$  ions/cm<sup>2</sup>), the polymer degrades its mechanical strength and as a result the hardness decreases. Still at higher fluence i.e.  $10^{15}$  ions/cm<sup>2</sup> the sample become dark brown and it was not possible to see the indentation mark.

#### **4.6.5 Surface Morphology**

The modifications in surface morphology are found with the change in colour of polymeric blend, which is dull Gray for the pristine film and no appreciable change in colour has been observed at the fluence of  $10^{13}$  ions/cm<sup>2</sup>. On further increase of the fluence the surface became yellowish-brown and dark brown at the fluence of  $10^{14}$  and  $10^{15}$  ions/cm<sup>2</sup> respectively. When these polymers were viewed through optical microscope it is observed

that the irradiated samples do not appear to be flat (smooth), but seem to be rough. The roughness of the sample increases as fluence increases.

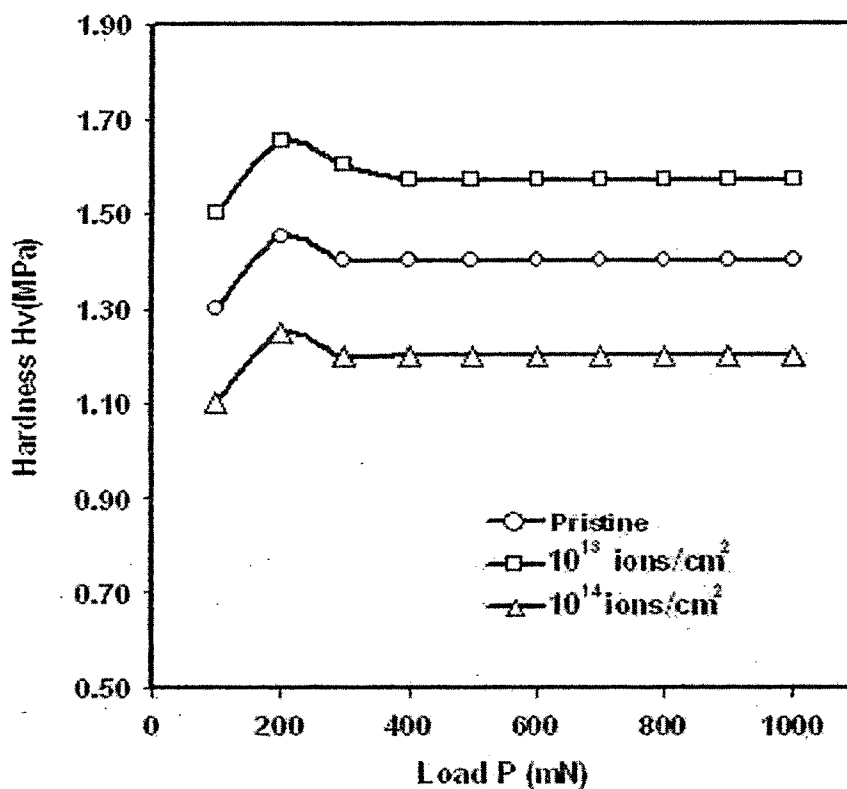
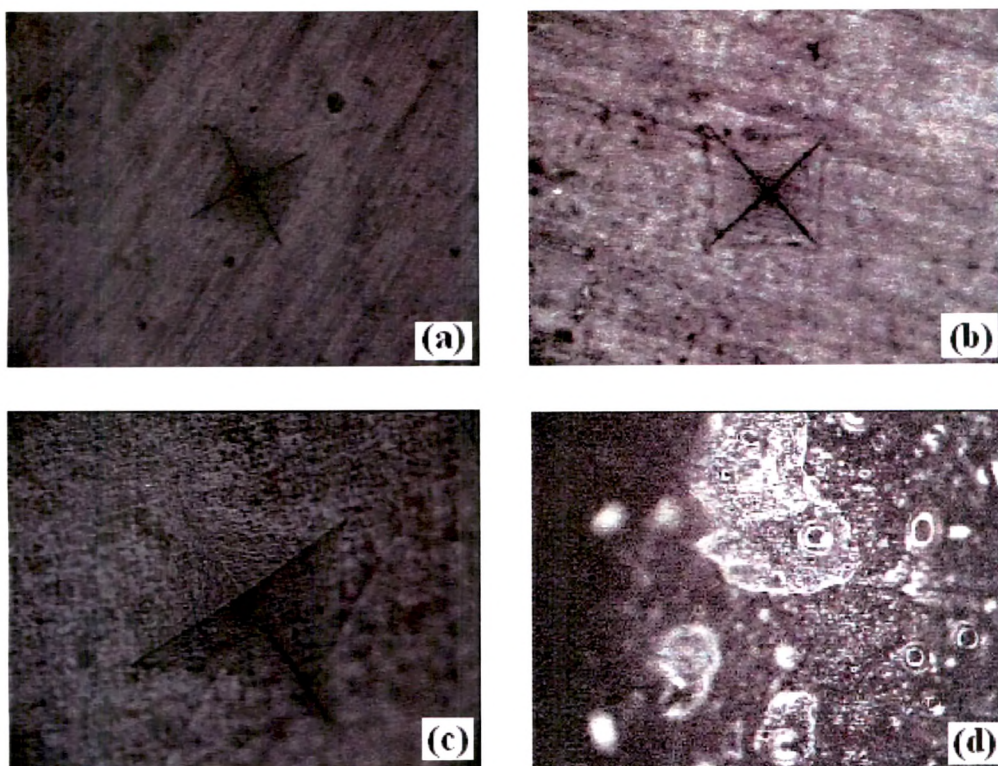


Figure 4.49: Microhardness for pristine and irradiated blend polymer films.

#### 4.6.6 Conclusion

The proton irradiations of blended polymers lead to chain scission and as a result there are changes in the dielectric properties. There is an exponential increase in conductivity with log frequency and the effect is significant at higher fluences. The DSC measurement of irradiated blended polymer shows significant changes in its melting property. This indicates that the melting temperature first increases with the fluence, and then decreases again. When ion track overlapping sets in, competing processes such as amorphisation

overtake, leading to a reduction of the melting point. The TGA thermogram indicates a degradation of the polymer matrix under proton irradiation making it to decompose earlier than the pristine sample, which is also corroborated by FTIR spectra. However, chain scission by proton irradiation at higher fluence seems to be the dominant process. The Vickers' microhardness of the blend polymer increases up to the fluence of  $10^{13}$  ions/cm<sup>2</sup>, probably due to cross-linking without any degradation effect. However, the Vickers' hardness decreases at the fluence of  $10^{14}$  ions/cm<sup>2</sup> because of degradation of polymer due to scissioning of polymeric chains, which is also corroborated by the FTIR spectra. Due to severe damage of surface at highest fluence microhardness indentation could not be measured. The optical micrographs indicate that the irradiated samples do not appear to be flat (smooth). It became rough and the roughness of polymer increases as the fluence increases.



**Figure 4.50: Optical micrographs of pristine and irradiated blend polymer films (a) pristine, (b)  $10^{13}$  ions/cm<sup>2</sup>, (c)  $10^{14}$  ions/cm<sup>2</sup> and (d)  $10^{15}$  ions/cm<sup>2</sup>.**

## REFERENCES

- [1] N Bohider, J. T. R. Chem. 1 (1994) 31.
- [2] G H Wang, G Q Pan, L Dou, S T J Zhang and L Q Dai Nucl Instr and Meth B 27 (1987) 410.
- [3] R Mishra, S P Tripathy, D Sinha, K K Diwivedi, S Ghosh, D T Khathing, M Muller, D Fink, W H Chung, Nucl. Instr. and Meth B 168 (2000) 59.
- [4] R Mishra, S P Tripathy, D Sinha, K K Diwivedi, S Ghosh, D T Khathing, M Muller, D Fink, W H Chung, Rad. Meas. 33(2001) 845.
- [5] Nilam Shah, N L Singh, K P Singh and D G Rathod, Indo German workshop on Synthesis and Modification of Nanostructured Materials by Energetic Ion Beams (2005) 79. (To be published in Nucl. Instr. Meth. B).
- [6] A K Jonscher, Review Article, Nature, 267 (1977) 673.
- [7] N P Bogoroditsky, V V Pasyukov, B M Tareev, Electrical engineering materials, Mir Publisher Moscow (1979).
- [8] M Mujahid, S Gupta, D K Avasthi and D S Srivastava, Proceedings of the Solid State Physics Symposium 42 (1999) 599.
- [9] A Broido, J. Polym Sci., 7(1969)1761.
- [10] X L Xu, Yu Yulhui, Lin Zixin, Chen Lizhi, Fung Fong, Zhore Zuyao and Zoci Shichang, 1991. Nucl. Instr. and Meth. B 59/60, 1267-1270.
- [11] D Fink, F Hosci, H Omichi, T Sasuga, L Amaral, Rad.Eff. Deff. In Solids 132 (1994) 313.
- [12] T Terai and T Kobashi, Nucl. Instr. and Meth. B166-167 (2000) 627.
- [13] Garg, M., Kumar, S., and Quamara, J.K., Ind. J. of Pure and Appl. Phys. 39 (2001) 455.
- [14] H S Virk , P S Chandi, and A K Srivastava, Bull. Mater. Sci 24 (2001) 529.
- [15] R Mishra, S P Tripathy, K K Dwivedi, D T Khathing, S G Ghosh, D Fink, Rad. Meas. 36 (2003) 719.
- [16] Nilam Shah, N L Singh, C F Desai, K P Singh, Rad. Meas. 36 (2003) 699.
- [17] N L Singh, Nilam Shah, P K Mehta, K P Singh, A K Rakshit, Jr. Thermal analysis and calorimetry (communicated).
- [18] E H Lee, G R Rao, L K Mansur, Mater. Sci. Forum, 248-249 (1997)135.
- [19] S K Awasthi, and R Bajpai, Ind. J. of Pure and Appl. Phys: 39 (2001) 795.
- [20] K Ciesla, W Starosta, Nucl. Instr. and Meth. B105 (1995) 115.
- [21] T. Steckereiter, E Balanzat, H Fuess, C Trautmann, Nucl. Instr. and Meth. B131 (1997) 159.
- [22] A Biswas, S Lotha, D Fink, J P Singh, D K Avasthi, B K Yadav, S K Bose, D T Khathing, A M Avasthi, Nucl. Instr. and Meth. B 159 (1999) 40.
- [23] S Tripathy, R Mishra, K K Dwivedi, D T Khathing, S Ghose, D Fink, Rad. Effec. and Deff. in Solids 157 (2002)387.

- [24] N L Singh , Nilam Shah, C F Desai, K P Singh and S K Arora, Rad. Effects and Defects in Solids 159 (2004) 475.
- [25] N L Singh, Nilam Shah, K P Singh, A K Rakshit, Proceedings of the Fourteenth National symposium on Thermal analysis (2004) 213.
- [26] A K Srivastava and H S Virk, Bull. Mater. Sci. 23 (2000) 533.
- [27] L Calcagno, P Musumlei, R Percolla and G Foti, Nucl. Instr. and Meth. B 91 (1994) 461.
- [28] Y Q Wang, L B Bridwell, R E Giedd, M.J Murphy, Nucl. Instr. and Meth. B 56/57 (1991) 660.
- [29] L B Bridwell, R E Giedd, Y Q Wang, S S Mohite, T Jahnke, I M Brown, C J Bedell and C J Sofield, Nucl. Instr. and Meth. B56/57 (1991) 659.
- [30] A L Evelyn, D Ila, R L Zimmerman, K Bhat, D B Poker, D K Hensley, C Klatt, S Kalbitzer, N Just, C Drevet, Nucl. Instr. and Meth. B148 (1999) 1141.
- [31] Nilam Shah, N L Singh, K P Singh, Rad. Effects and Defects in Solids (Communicated).
- [32] E Ferain and R Legras, Nucl. Instr. and Meth. B82 (1993) 539.
- [33] Steckenreiter T, Balnzat E, Fuess H and Trautmann C, Nucl. Instrum & Meth. B 151 (1999) 161.
- [34] L Piraux, S Dubois, J L Duvail, A Radulescu, S Demoustier-Champange, E Ferain, R Legras, J. Mater. Res. 14 (1999) 3042.
- [35] F Dehaye, E Balanzat, E Ferain, R Legras, Nucl. Instr. and Meth. B209 (2003) 103.
- [36] Y Wang, Y Jin, Z Zhu, C Liu, Y Sun, Z Wang, M Hou, X Chen, C Zhang, J Liu and B Li Nucl. Instr. And Meth. B164/165 (2000) 420.
- [37] Z Zhu, Y Sun, C Liu, J Liu, Y Jin, Nucl. Instr. and Meth. B193 (2002) 271
- [38] M I Chipara and J Reyes-Romero Nucl. Instr. and Meth. B185 (2002) 77.
- [39] N L Singh, Nilam Shah, K P Singh, Bull. Mater. Sci. (In Press).
- [40] N L Singh, Nilam Shah, S Mukherjee and K P Singh, Proceedings of 22<sup>nd</sup> International Conference on Nuclear Tracks in Solids (2004) 258. (Rad. Meas.-in press).